POWER LINE COMMUNICATION IMPEDANCE PROFILING AND MATCHING FOR BROADBAND APPLICATIONS

by
Florence Chelangat

Dissertation submitted in fulfilment of the requirement for the degree
MASTER OF SCIENCE IN ENGINEERING: ELECTRONIC ENGINEERING
in the
School of Engineering

UNIVERSITY OF KWAZULU-NATAL

Supervisor: Prof. Thomas Joachim Odhiambo Afullo

Co-Supervisor: Dr. Modisa Mosalaosi

EXAMINER'S COPY

June 2018

As the candidate's supervisors, we have approved this dissertation for submission.

Signed .....Date .....

Name: Prof. Thomas J. O. Afullo

Signed .....Date .....

Name: Dr. Modisa Mosalaosi

Declaration 1 - Plagiarism

I, **Florence Chelangat**, declare that

1. The research reported in this dissertation, except where otherwise indicated, is my original research.
2. This dissertation has not been submitted for any degree or examination at any other university.
3. This dissertation does not contain other persons' data, pictures, graphs or other information, unless specifically acknowledged as being sourced from other persons.
4. This dissertation does not contain other persons' writing, unless specifically acknowledged as being sourced from other researchers. Where other written sources have been quoted, then:
   (a) Their words have been re-written but the general information attributed to them has been referenced
   (b) Where their exact words have been used, then their writing has been placed in italics and inside quotation marks, and referenced.
5. This dissertation does not contain text, graphics or tables copied and pasted from the Internet, unless specifically acknowledged, and the source being detailed in the dissertation and in the References sections.

Signed .....Date .....

Declaration 2 - Publications

List of publications related to this Dissertation including their overlapping Chapters:

1. Overlapping Chapter 4
   F. Chelangat, Thomas J. O. Afullo, and M. Mosalaosi, "Impedance modelling profiling and characterisation of the power line communication channel," in *Progrees in Electromagnetic Research Symposium (PIERS)*, Toyama, Japan, Accepted to be presented in 1-4 August, 2018.

2. Overlapping Chapter 5
   F. Chelangat, Thomas J. O. Afullo and M. Mosalaosi, "Impedance Bidirectional Adaptive Coupler for Broadband PLC," *Submitted to Proceedings of Southern Africa Telecommunication Networks and Applications Conference (SATNAC)*, 2018.

Signed .....Date .....

Acknowledgements

I would like to thank God for the good health, peace of mind and seeing me through this research. I would also like to express my sincere gratitude to my supervisor Prof. Thomas J. O. Afullo and my co-supervisor Dr. M. Mosalaosi for the invaluable insights on my research area, priceless mentorship and support throughout my period of study. For this I will be forever indebted. The opportunity to explore and develop this work has been truly rewarding. I strongly believe that the contribution made in this research will go a long way in the field of powerline communications.

I would also like to thank my collegues Mr. Steven Awino, Madam Mary Nabangala and Mr. Nicholas Oyie for the role they played in the academic research and my stay in Durban. I would especially like to acknowledge Mr. Steven Awino for his assistance and handling of the PLC equipment and Mr. J. Mpisi (Lab Technician) for his support and giving me the components required for my research.

Finally, I wish to express my sincere gratitude to my mom and dad, Mr. Joseph Biwott Chemirmir and Mrs. Priscila Biwott, my sisters Chepng'eno, Chepkoech and Cheptoo and my brothers Victor and Brian for their unconditional love, care and support throughout out my life. You have been my biggest cheerleaders. I also would like to thank the entire Chemimir's family for their unwaivering support and raising me to be the great lady I am today. I would also like to extend my sincere appreciation to my fiancè Stephen Lewis Opot for all the support and encouragement all through my research period.

May God bless you all abundantly and may you never lack.

Abstract

Power line communication(PLC) is a wired communication technology that has recently received a lot of attention due to its attractive prospects towards home and /or neighborhood network applications as well as smart grid technologies. It allows establishing digital communications without any additional wiring requirements. Effectively, one's home and/or neighborhood wiring contributes into a smart grid to deploy various data services. It is well known that the power grid is one of the most pervasive infrastructure built to provide electricity to customers, therefore, utilizing this infrastructure for digital communications will only result in an ubiquitous telecommunications network. It is common practice to use wires to establish a physical connection in many telecommunications channels, but most electronic devices already have a pair of wires connected to the power lines. Therefore, these wires can be used to simultaneously establish digital communications. Thus, power line communications can be used as an alternative solution to more established technologies such as wireless, coaxial and optical communications. As a promising technology, PLC has attracted a lot of research and has become an active area of research which continues to evolve over time. Notwithstanding its advantages, PLC has issues, namely, severe noise at low frequencies and varying characteristic impedance. This is primarily because the power line channel was not originally designed to be used for communications, thus, it remains a harsh channel. Other challenges arise from the fact that there are different wiring practices around the world, unpredictable loading characteristics as well as differential- and common-mode characteristic impedance. As a result, there is a considerable amount of noise signal attenuation during data transmission. Loss of signal can be addressed by increasing the power at the transmitter, noise reduction and/or reducing channel attenuation to improve the signal-to-noise ratio. However, PLC modems are subject to legislation that impose a limit with regards to the signal levels in the lines. Power lines are good radiators at high frequencies which makes them behave like large antennas with the ability to intercept other radiations in the same frequency range. The radiated signal is proportional to the currents in the line, thus, increasing line currents will not solve the problem but would rather lead to violation of electromagnetic compatibility (EMC) regulations.

In this work, an alternative solution is provided which seeks to address the issue of signal attenuation caused by the changing input impedance of a typical power line channel. The deleterious effects of noise are not considered since this work focuses on broadband PLC in the 1–30 MHz frequency range. The objective of this work was to design and build an impedance adaptive coupler to mitigate effects of channel attenuation caused by varying impedance. In this way, the propagating signal will "see" a uniform impedance and as a result the data output will be improved. The work was facilitated by measuring several impedance profiles of PLC channels in the band of interest. Typically, the network topology of PLC networks is not known and the building architectural blueprints are

not always readily available. To overcome this issue,this work was performed on power line test-beds designed to mimic varied typical PLC network topologies. Moreover, there is an additional benefit in that it is possible to relate the output impedance profile to the network topology. The channel input impedance characteristics were determined in a deterministic manner by considering a power line network as a cascade of parallel resonant circuits and applying transmission line theory to develop the model. The model was validated by measurements with good agreement over the frequency range was considered. Several measurements were then used to determine the minimum, average and maximum input impedance that a signal will experience as it traverses the channel. It was found that, regardless of the network size (in terms of number of branches), the average input impedance is $354 \pm 1.1\ \%\ \Omega$ in the 1-30 MHz frequency band. Due to the unpredictable nature of the input impedance of the power line network, an impedance adaptive bidirectional coupler for broadband power line communications was designed. The impedance matching is achieved by using typical L-section matching networks in the 1–30 MHz band. The matching section of the coupler has the characteristics of a lowpass filter while the coupling section is a highpass filter, effectively forming a bandpass network. The simulated transfer characteristics of the designed coupler performs very well for impedances starting around 150 Ω and the performance improves a great deal as the impedance increases. The coupler can still be improved to accommodate much lower input impedances (as low as 50 Ω). However, based on the measured results of input impedance, it was observed that the power line channel impedance is statistically higher than 200 Ω most of the time which makes the presented design acceptable.

Contents

List of Figures

List of Tables

Chapter 1

INTRODUCTION

1.1 Power Line Communication (PLC) Background

The demand for digital telecomunication access and services to almost every premise has tremendously increased since the introduction of the internet in the 1990's, the intranets and extranets [1]. The telecommunication sector particularly evolved the modes of communication as businesses changed their mode of service delivery to their customers through the use of online platforms such as billing applications and also in the exchange of information. This has led to the need for cost effective and efficient alternative solutions for communication services. Power line communication comes in handy to fill this gap. A lot of research has therefore been undertaken, on the use of the power line network for data transmission due to its extensive coverage and readily available infrastructure.

PLC network is pervasive since every building existing and yet to be constructed will have electrical connectivity. In addition, there is lower maintenance cost of PLC networks, for example, the replacement of the power line cables is much more affordable than the replacement of devices such as cables, switches and outlets used in other conventional data communication systems [2]. Therefore, power line communication compared to other wireline alternatives such as telephone loops, ethernet, and fibre optical cable, is the only technology whose deployment cost is comparable to wireless technologies [3]. Furthermore, PLC presents an ideal physical medium for data communications as the power line infrastructure coverage by far exceeds that of the digital infrastructure and will play an important role in minimizing the digital divide in developing countries [4, 5].

PLC systems are divided in to two main categories depending on the frequency band of operation, with the band 3–500 kHz used for narrowband and 1 MHz–300 MHz for broadband applications [6, 7]. Automatic meter reading and load control were among the first aplications of PLC using single carrier narrowband solutions that attained data rates ranging from few bits per second (bps) to a few kilobits per second [8–11]. Despite the hostile nature of the power line channel such as noise and impedance variation towards high frequency communication signals, its capacity has been found to exceed 3 Gbps when the distance between the transmitter and receiver is below 10 m for a frequency bandwidth of 0–300 MHz [6]. Therefore, the provision of of high-speed and low-speed vehicular communication was investigated by various researchers [6, 7, 12]. Other applications of PLC include home automation in controlling the lighting, sensors for alarm systems and other appliances, home networking and internet access and radio broadcasting [13–15].

1.2 PLC Historical Overview

The use of power line technology was first proposed by Edward Davy in 1838 for the purpose of monitoring the voltage levels of batteries at unmanned sites in London [1]. It was not until 1910, when the transmission of analog signals over a single telephone circuit using carrier-frequency techniques was demonstrated by Major George Squier of US Army [16, 17]. In May 1918, the carrier telephony over power lines was successfully tested in Kinogawa Hydro-Electric Co. over a 144 km long power line. Later that year, the first commercial operation of the "wired telephony" over a 22 kV 3-phase power line was done by Fuji Hydro-Electric Co. [18]. This then motivated for more telephone communications over the power line experiments to be done and in 1920, the American Gas & Electric Co. reported successful transmission of communication signals over live high-tension lines. The report even recommended that PLC would ensure a reliable and more affordable mode of communication between its load dispatchers and interconnected stations [16].

After the success of these experiments, other power companies began installations since telephone coverage in those years was very poor especially during winter storms. PLC technology provided a better alternative way of communication for operations management with colleagues stations at different power stations tens or hundreds of km away as well as synchronization and energy distribution [11, 16]. Thus, the use of carrier frequency telephony over power lines had widely spread through out Europe and the United States [19]. The 1930s were characterized by the use of ripple carrier signalling to control heavy duty appliances such as water heaters and air conditioners that consumed high amounts of energy. This was achieved by issuing control signals to switch on/off the appliances via the power line network. Other applications of the ripple carrier signalling included street light control, day/night tariff switching and control of equipment on the power grid [10, 11, 20, 21].

The progress in PLC communication was significant by the late 1980s, with development of sophisticated error control coding techniques within the hardware of the PLC modems. Electrical power grids also showed potential as a medium for data communication for a frequency bandwidth of 5 kHZ–500 kHz [22, 23]. Due to the growing demand for higher data rates, CENELEC issued EN 50065 standard that allowed communication over low voltage distribution power lines in the frequency range of 3 kHz–148.5 kHz. In this band, 3–95 kHz was exclusively reserved for power utilities, 95–125 kHz for any application, 125–140 kHz for in-home networking systems with a mandated carrier sense multiple access with Collision Avoidance Protocal and 140–148.5 kHz was reserved for alarm and security systems [24]. Other countries such as the United States and Asia allowed for operation of upto 500 kHz.

The progress in the narrowband PLC applications gave rise to the use of frequencies above 1 MHz for internet access applications and successively for home area networks (HAN) and audio/video applications. However, the broadband PLC was limited to a frequency bandwidth of 1–30 MHz with some constraints on the transmission power and distance [25]. PLC, after demostrating a technical feasibility for the transmission of high frequency

signals on the low voltage lines, formally joined the family of broadband communication systems in 1995 [26].

1.3 Power line Distribution Network

PLC as its name suggests, utilizes the electrical infrastructure as its medium for transfer of communication signals. Ideally, the power line network was conceived for the transmission and distribution of 50 Hz or 60 Hz AC power signals from the generating stations to the consumer depending on the country. Therefore, unlike other conventional media of communication such as coaxial cables, optical fibre and and ethernet cables, the power line network differ in structure, physical properties and topology. This necessitates for the understanding of the power line network so as to verify its viability and its challenges as a communication medium. The power line is divided in to three classes depending on the voltage levels as high-voltage level (110–330kV), medium-voltage level (10–30kV) and low-voltage level (0.4kV) interconnected together through transformers [10]. These interconnecting transformers allow only the low frequency electrical signals to pass through while blocking the high frequency signals. A typical electrical power grid is as shown in Figure 1.1

1.3.1 High-voltage Transmission lines

After generation, electrical power is transmitted via high-voltage power line to multiple substations, traversing over long distances of upto several hundreds of kilometers. Electrical power is transmitted through three phase conductors at high-voltage in order to minimize energy loss in long distance transmission. However, there still remain some losses

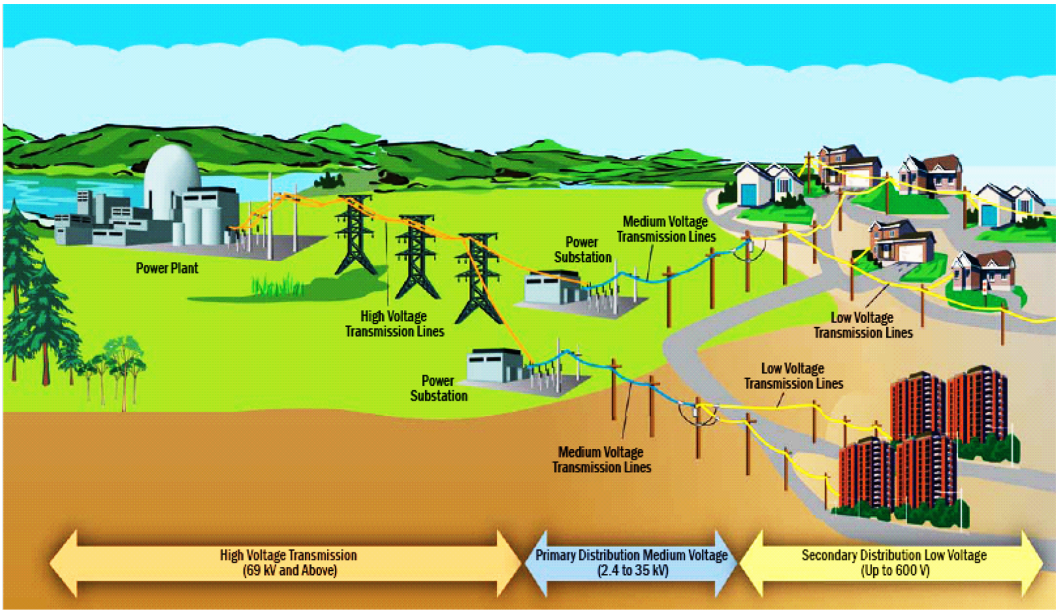

Figure 1.1: Electrical power grid [http://file.scirp.org/Html/2 – 9701842$_4$9419.htm]

in the high-voltage lines with heat loss being the major loss and is caused by resistance of the power line material and leakage losses. In order to minimize heat losses to acceptable levels, a proper dimension and a good selection of the wire material of the transmission lines is essential. The heat losses may also be reduced by increasing the nominal voltage but this would also lead to an increase in the leakage losses [10].
High-voltage transmission lines also suffer from corona losses due to discharge activities in the vicinity of the conductors as a result of the high electric field strengths at high voltages. Corona losses become even more severe if thinner conductors are used for the transportation of high-voltage signals. Corona losses lead to energy losses and can produce intensive high frequency impulses that interfere with radios using low and medium frequency bands and therefore need to be reduced. This can be achieved through proper geometric arrangement of the high-voltage wires [10].
High-voltage overhead transmission lines though good waveguides, present periodic-short duration impulsive interference that arise from switching events and atmospheric discharges resulting in high impulses that cause dangerous peaks at the receiving end. High-voltage transmission lines also posses permanent broadband interference which has a fairly high power spectral density (PSD) that strongly depends on the weather conditions and tends to be severe when there is rain, frost or fog. This permanently present broadband interference can be modeled as white Gaussian noise and results from discharge activities. All in all, high-voltage lines are a much better communication medium compared to low-voltage and medium-voltage lines. However, alternative communication technologies which allow higher data rates such as fiber optical and microwave links may be used if available [11]. PLC over high-voltage lines is also useful in remote fault detection and in the determination of the average change in height of the horizontal high-voltage overhead lines [27].

1.3.2 Medium-voltage Transmission lines

The medium voltage line basically forms a link between the high-voltage and the low-voltage transmission lines. They supply electrical power to the small towns, rural areas and individual manufacturing companies. The medium -voltage transmission lines can either be used as overhead lines or underground cables. In densely populated areas such as cities, the underground cables are preferred due to many tall buildings that characterize the urban areas. Medium-voltage lines transmit voltages ranging from 10–30 kV over a distance between 5–25 km and therefore relatively small poles and smaller wire cross-sections are used in comparison to the high-voltage lines [10]. Medium-voltage lines are majorly composed of copper and aluminium with varied cross-section shapes that include sector-shaped, oval and round [10]. Polyvinyl Chloride or vulcanized polythelene is normally used as the insulation medium. PLC over the medium-voltage has been used to measure temperature of oil transformers, faults surveys, voltage measurement on the secondary winding of high-voltage/medium-voltage transformers and power quality measurements [28].

1.3.3 Low-voltage Transmission lines

The low-voltage network form the last part of the electrical power line network and supply 100–400 V electrical power to consumers [10]. The low-voltage power lines extend a distance of 500 m from the medium-voltage/low-voltage transformer to the consumer's premises. Similar to the medium voltage networks, both underground and overhead lines are used. The physical structure, composition and insulation materials of the low-voltage transmission lines is the same as that of the medium-voltage lines. Some of the PLC applications in the low-voltage lines include automatic meter reading, vehicle-to-grid communications and management of indoor energy [11]. It is at the low-voltage level that various appliances are connected to the power line grid and thus the PLC network. A typical connection of the PLC network is as shown in Figure 1.2.

1.4 PLC Standards and Regulations

Standards are of paramount importance in PLC as they ensure efficient transparent communication over the power line network. Standards in PLC also allow for a large-scale economic implementation and as such many countries come together to find a common ground as in the European Union. However, the USA is content with having its own separate standard that is probably motivated by its large market which is enough to develop and maintain the technology. The PLC standards are responsible in defining the frequency bands, emission limits and background noise, measurement standards including coupling as well as the maximum modem output levels [29]. Standardization organizations (SDOs) focus on the physical (PHY) and the data link layers (DLL) of the PLC network [5, 30]. In order to simplify and provide fair regulations the the PLC standards have been

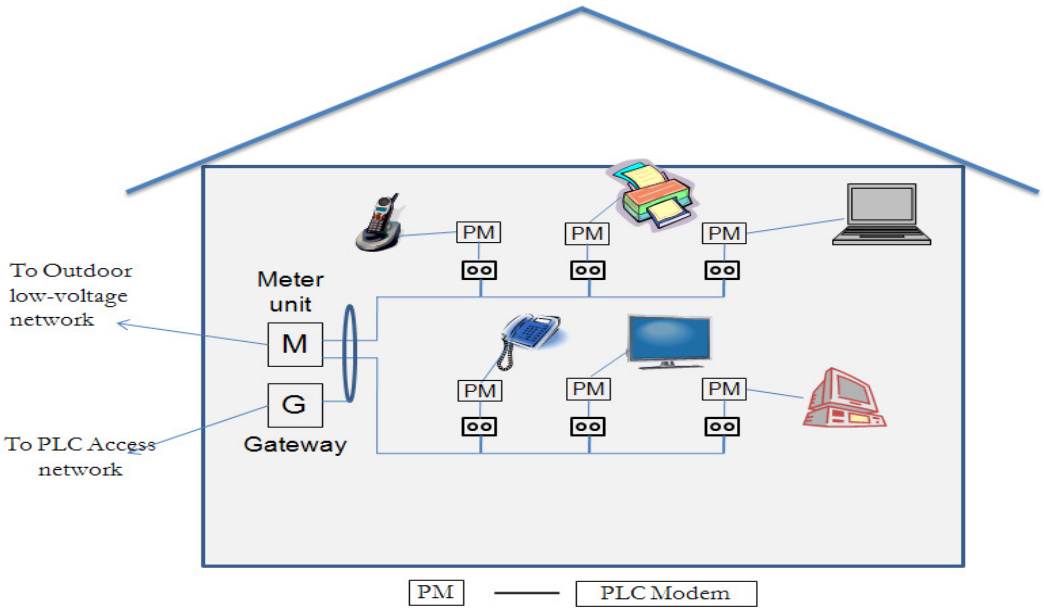

Figure 1.2: PLC indoor network [https://www.researchgate.net]

defined based on the frequency bands as narrowband PLC (NBPLC) for frequencies below 500 kHz and broadband PLC (BBPLC) for frequencies above 1 MHz.
SDOs in PLC are categorized into two groups: those that develop and propose standards and those that develop and deploy standards and technologies in the PLC sector. The SDOs in the former group include international telecommunication union (ITU), the international organization for standardization (ISO), the international electrotechnical commission (IEC), the institute of electrical and electronic engineers (IEEE) and the European committee for electrotechnical standardization (CENELEC). Some of the SDOs that fall under the latter group include G3-PLC, power line intelligent metering evolution (PRIME), the american national standards institute (ANSI) and HomePlug [30].
The EN 50065 standards in Europe specifies NBPLC to work in the range of 3 kHz–148.5 kHz while IEEE and ITU propose 9–500 kHz and 2–490 kHz, respectively. The PRIME, ANSI and G3-PLC are specified for working in the CENELEC frequency band over the NBPLC networks. The HomePlug network specifies 120–400kHz for the NBPLC application. The NBPLC can offer data rates upto 500 kbps in using the orthogonal frequency division multiplexing [31]. The PLC frequency allocations by various SDOs for both the narrowband and bandbroad PLC are as shown in Figures 1.3 and 1.4 [30].

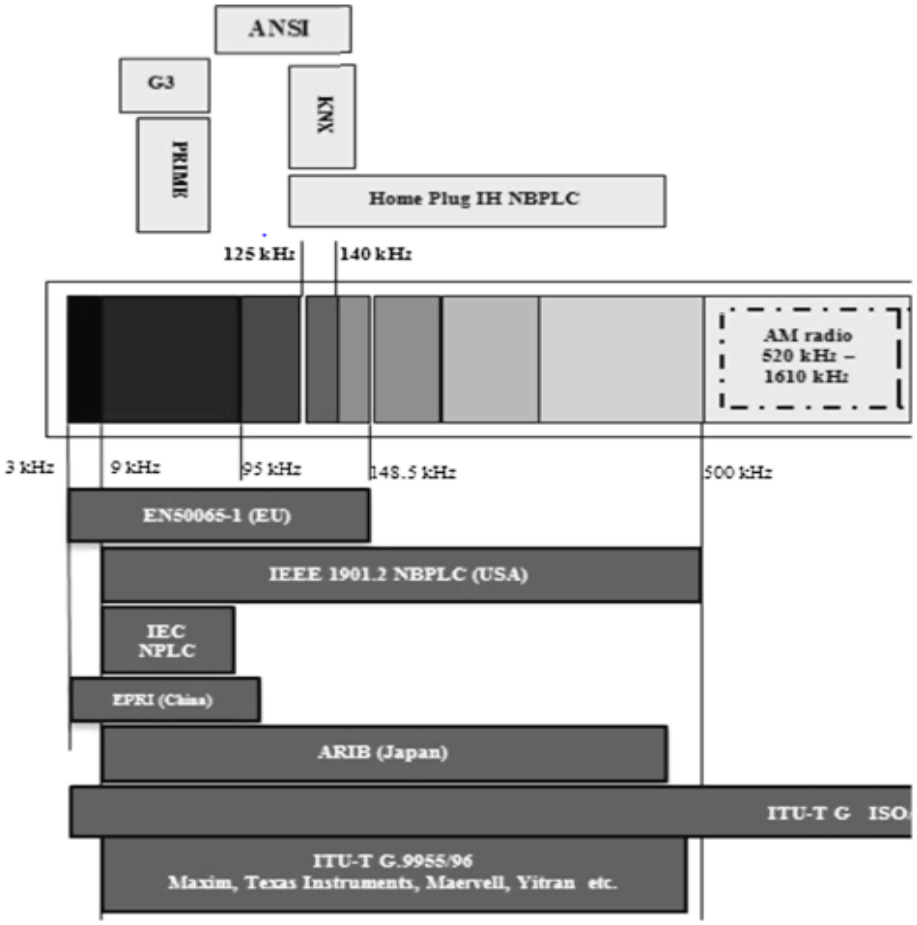

Figure 1.3: NBPLC frequency allocation [30]

In the BBPLC two worlwide standards have been defined, namely ITU-T G.hn (ITU-T

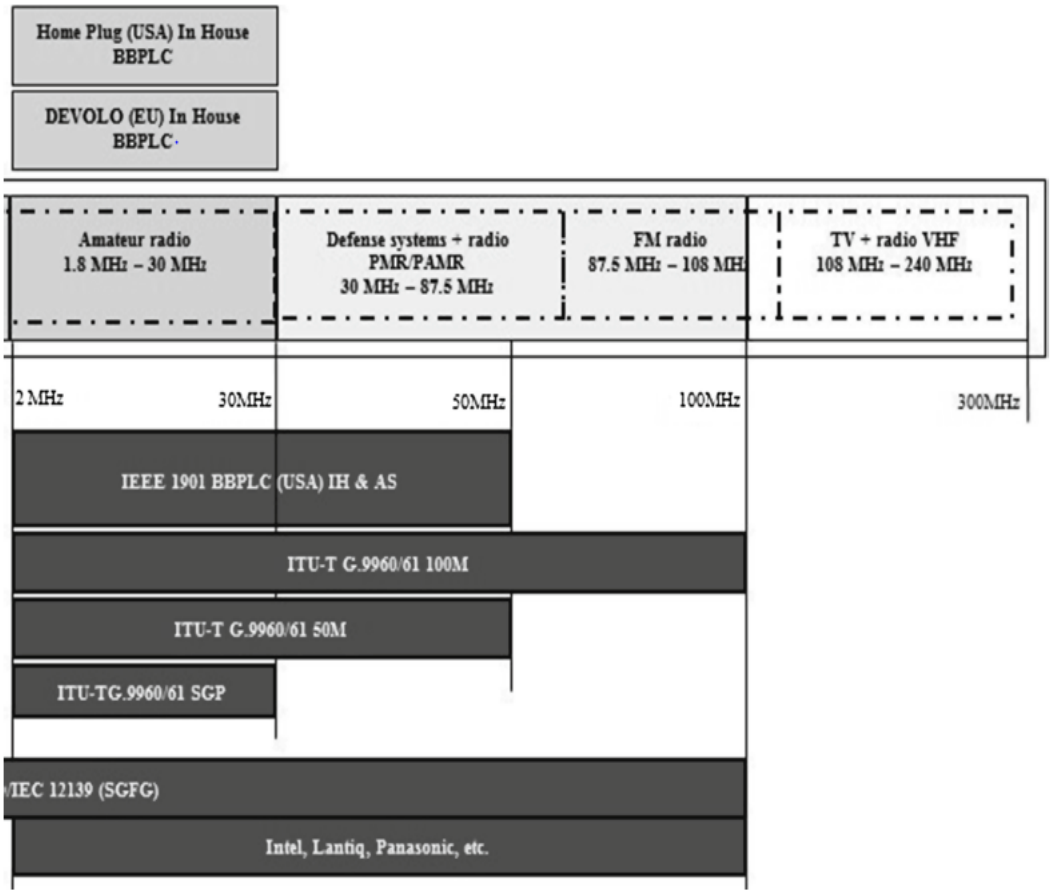

Figure 1.4: BBPLC frequency allocation [30]

G.9960) and IEEE P1901 (IEEE 1901-2010). Therefore, technologies in broadband can operate at frequencies between 1.8–86 MHz and can potentially reach data rates of upto 1 Gbps in home networks. The HomePlug on the other hand has defined the HomePlug Green PHY specifications in the 1.8–30 MHz for energy efficient transmission [31]. In this research, analysis and investigations have been conducted for BBPLC for the 1–30 MHz band.

1.5 PLC Limitations

The original purpose of the power line network was to transmit high voltage low frequency electrical signals from the generating stations to the consumers. Therefore, transmitting high-frequency signal results in highly unpredictable attenuation, electromagnetic interference, power line impedance and noise that change their values with frequency, time and location.

1.5.1 Attenuation

As the communication signal travels from the high-voltage, through medium-voltage and the low-voltage to the consumer, it losses it signal strength due to corona losses and leakage losses in the transmission lines. The different characteristics of the distribution lines also lead to the variation in attenuation. The attenuation also varies with frequency such that a signal transmitted at high frequency for example 10 MHz will be highly attenuated as compared to a signal transmitted at 100 kHz. This is due to the fact that the skin effect will cause the effective conductor area to reduce by approximately 10 times since the frequency is higher by a factor of 100 [32].

1.5.2 Varying impedance

The low-voltage indoor in networks residential areas are heavily branched with each branch having a different signal attenuation level as different rooms may contain more than one socket outlets. Thus, at each branch node, there are multiple signal reflections of the propagation signal leading to variation in power line impedance [33,34]. Moreover, at each outlet, different loads are connected and disconnected randomly resulting in impedance fluctuation. As a result, only a fraction of the transmitted signal will be available at the receiver and also make impedance matching a nontrivial task [35].

1.5.3 Noise

PLC noise is one of the major challenges in the transfer of data through the power line channel. The switching on and off of the loads in the low-voltage networks not only results in impedance fluctuation but also generate noise that is superimposed onto the data signal in the PLC channel. In addition, lightning strikes, low-level corona discharges,circuit breaker transients and other atmospheric discharges causes noise in high-voltage and medium-voltage level of the power line network. [5].

1.5.4 Radiation

The signal is injected by a PLC modem into the power line network via differential mode. However, part of the differential mode is converted to the parasitic common mode due to asymmetries in the power line structure, non-purely differential loads and electrical imbalances of the PLC modems [36]. As a result the PLC network produces radiated electromagnetic field which interferes with radio communication services operating in the same band [37,38]. In addition, PLC cables act as good antennas at high frequencies and therefore radiate and intercept radios sharing the same frequency band.

1.6 Research Objectives

PLC has recently received a lot of attention due to its attractive prospects towards "last mile" network applications as well as smart grid technologies and is therefore an active area of research. Although PLC is a promising technology, it is faced with challenges that include varying and fluctuating input impedance, high signal reflection and noise. This work focuses on the input impedance of the PLC network. The power line impedance posses different properties depending on the frequency. Many works and have been done on the improvement of the input impedance through matching for the narrowband PLC network. This has not been the case for broadband PLC. This work seeks to investigate and address the issue of signal attenuation caused by the changing input impedance of the broadband PLC channel.

The objectives of this study are as follows:

- To perform measurements on a test-bed to determine the characteristics of the input impedance of the PLC network in the band 1–30 MHz.
- To characterize and profile the measured input impedance for the known network topologies and determine the minimum,average and maximum values.
- To model the PLC input impedance and compare the proposed model with measurements for different network topologies.
- To design and build an impedance adaptive coupler to mitigate the effects of highly varying impedance.
- To test the performance of the matching coupler under different loading conditions.

1.7 Thesis Organization

This dissertation consists of six chapters and begins with chapter 1 where we present the PLC background. This chapter also discusses the history of the PLC upto the current advancement in the technology. The power line distribution network which is the backbone of the PLC is described and the various standards and regulations are reviewed. In chapter 2, the review of the major powerline channel models, transmission line theory and the methods of impedance matching are presented. The extraction of line parameters used in the PLC modeling is discussed in chapter 3. Chapter 4 focuses on the modeling, characterization and profiling of the powerline input impedance. In chapter 5, the impedance matching coupler design is presented and its performance under various loading conditions discussed. The research findings of the dissertation are concluded in chapter 6 as well as recommendations for future work.

Chapter 2

LITERATURE REVIEW

2.1 Introduction

To date, there has not been any universally accepted model for the PLC channel. This is due to its diverse characteristics and topologies that vary from country to country [39, 40]. Moreover, the wiring practices vary significantly depending on the area and population [41]. The power line network, for example, will be heavily branched in a densely populated area as compared to scarce populations resulting in increased signal reflection. The transfer function of the PLC channel is very important in determining the rate of signal attenuation, the choice of transmission technique, the capacity as well as the design parameters of the channel [42]. To that effect, various researchers have come up with models that help to give insight on the behavior of the PLC channel under different loading conditions. However, coming up with a model that incorporates all the measurements into a mathematical model, describes all the channel characteristics and maintain its simplicity such that any statistic required may be extracted while still remaining physically meaningful in terms of the distribution in both space and time is the greatest challenge in the characterization of the PLC channel properties. Due to the heterogeneous nature of the wiring practices, loads connected to the PLC network with unmatched impedance to the feed lines and branches connected to the network, impedance mismatch and fluctuation with time and frequency are a major challenge in the design of PLC modems and modeling of the power line channel characteristics. The need to mitigate these challenges has been of major interest in the quest to improve the transfer characteristics. In this chapter, the various PLC models have been presented to provide an insight on the PLC channel. In addition, the transmission line, in which the communication signal is transmitted has been analyzed. The effect of the PLC input impedance on the transfer function has been discussed. The improvement of the power line channel transfer function through various methods of impedance matching has also been discussed.

2.2 The Power line Channel Modeling

The power line network differs considerably in topology, structure and physical properties contrary to the twisted-pair, coaxial cables, fiber-optic cables and other wired communication mediums, thus presenting rather hostile properties to the PLC systems [43, 44]. Therefore, for planning of the PLC networks and appropriate communication systems to be designed, models of the transfer characteristics of the low voltage network are

required. In addition, the very complex channel characteristics of the PLC channel can be easily understood. Currently, there are two main approaches in the modeling of the PLC channels, namely top-down and bottom-up models [44–46]. In the top-down model, also referred to as the parametric approach, a channel model is developed and the channel parameters obtained from measurements which are then fitted into the the model. This approach has an advantage in that it is easy to implement and requires little computation. However, a large number of measurements is required for a good fitting to the actual channels to be realised and is also prone to measurement errors. In the bottom-up approach also referred to as the deterministic approach, a comprehensive knowledge of the components of the network and its physical structure is needed to model the channel transfer function. The deterministic approach is especially useful in addressing the the major causes of observed system behavior since the model parameters are clearly defined. In addition, it can be used to obtain statistically representative channels by the generation of random topologies [46]. The bottom-up approach however, requires increased computational efforts due to the large number of parameters introduced by the modeling matrices. If the values of some of the parameters are unknown, the characterization of the PLC channel will be significantly affected. There are several contributions in the modeling of the PLC channel. Some of the models that utilise the top-down approach include Zimmermann and Dostert multipath model [43], Philipps' series resonant circuit (SRC) model [47] and Philipps' echo model [47]. Models that represent the bottom-up approach include Meng et al. model [44], Anatory et al. model [48, 49], Esimilan et al. model [44], Zwane and Afullo SRC model [50] and parallel resonant circuit model [51, 52].

2.2.1 Philipps' Echo Model

The echo model regards the power line channel as a multipath environment where a signal transmitted not only reaches the receiver via a direct path, but also indirectly whereby it is delayed and in most cases attenuated. This is as a result of reflections that occur at impedance discontinuities such as branches and impedance mismatch causing echoes of the transmitted signal. This phenomenon is as shown in Figure 2.1.

Therefore, the receiver obtains signals through N paths and for each path, the complex

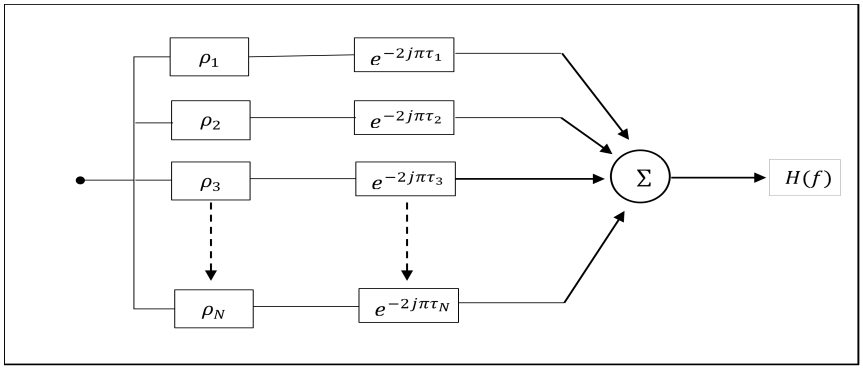

Figure 2.1: Echo Model [47]

attenuation is given by:

$$\rho_v = |\rho_v| e^{\jmath \phi_v} \tag{2.1}$$

where the signal on a path $_v$ is delayed by time τ_v, attenuated by a complex factor ρ_v and the phase-shift ϕ_v given by:

$$\phi_v = \arctan\left(\frac{Im(\rho_v)}{Re(\rho_v)}\right) \tag{2.2}$$

The impulse response h(t), is thus given by [47]:

$$h(t) = \sum_{v=1}^{N} |\rho_v| e^{\jmath \phi_v} \delta(t - \tau_v) \tag{2.3}$$

The transfer function is then derived from the Fourier transformation of h(t) and is desribed by three parameters, ϕ_v, ρ_v and τ_v obtained by an evolutionary strategy as [47]:

$$H(f) = \sum_{v=1}^{N} |\rho_v| e^{\jmath \phi_v} e^{-\jmath 2\pi f \tau_v} \tag{2.4}$$

2.2.2 Zimmermann and Dostert Multipath Model

The multipath model is developed from the echo model but in addition, it factors in the attenuation of the signal as it traverses through the line from the transmitter to the receiver. The PLC network is composed of numerous branches, joints, different characteristic impedance of the cable and loads are randomly plugged in and out of the PLC network and other points of impedance discontinuities [43]. Therefore, the transmitted signal is bound to suffer from multiple reflections as it does not only take one path, but also different paths to reach the receiver. Figure 2.2 is used to explain the multipath scenario. In Figure 2.2 the link has three segments (1), (2) and (3) with lengths L_1, L_2 and L_3 with characteristic impedances Z_1, Z_2, and Z_3 and consists of one branch B-D. A and C are assumed to be matched and thus $Z_A = Z_{L1}$ and $Z_C = Z_{L2}$ with points B and D as the only points of reflection. The reflection factors are denoted as r_{1B}, r_{3D} and the transmission factors are denoted as t_{1B} and t_{3B} at these points of discontinuities. Thus, the signal injected into the network can take various paths such as A-B-C, A-B-D-B-C, A-B-D-B-D-B-C and so on with each path i having its own weighting factor g_i, which is equal to the product of the reflection and transmission factors in that

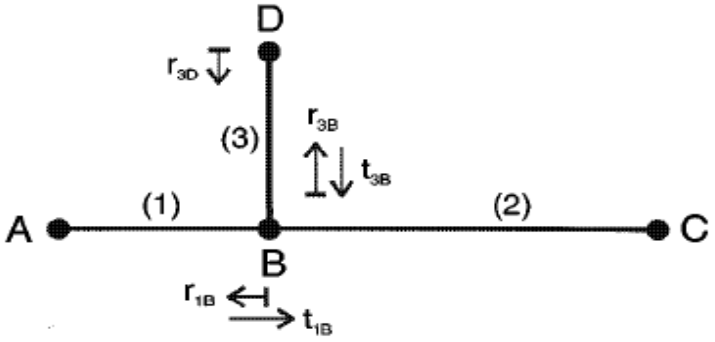

Figure 2.2: Multipath propagation for a single tap [43]

path. As the number of transmissions and reflections increase, the weighting factor reduces and the longer paths which exhibit high attenuation, thus the signal reaching the receiver contributes less to the overall signal. The complex channel transfer funtion of a multipath model is given by:

$$H(f) = \sum_{v=1}^{N} g_i . e^{-(a_o + a_1 f^k) d_i} . e^{j2\pi f \tau_i} \tag{2.5}$$

where N is the number of propagation paths, g_i the weighting factor, a_o, a_1 and k are the attenuation coefficients, d_i is the path length and τ_i the path delay given by:

$$\tau_i = \frac{d_i}{\upsilon_p} \tag{2.6}$$

where υ_p is the speed of propagation. The parameters of the channel are obtained from measurements.

2.2.3 Anatory et al. Model

In this model, the loads connected to the network, the number of nodes and their distance from the path line are taken into consideration. It considers a single node in a transmission line with multiple distributed branches and is based of the fact that at any particular node, part of a signal will be transmitted and the other part reflected. This scenario is a shown in Figure 2.3, where Z_s is the source impedance, Z_n the characteristic impedance of any terminal, V_s the source voltage and Z_l the load impedance. The transfer function of the model for any single node is then given by [48, 49, 53]:

$$H_m(f) = \sum_{M=1}^{L} \sum_{n=1}^{N_T} T_{LM} \alpha_{mn} H_{mn}(f) \qquad n \neq m \tag{2.7}$$

and the reference output voltage $V_m(f)$, across any load is given by [48, 49, 53]

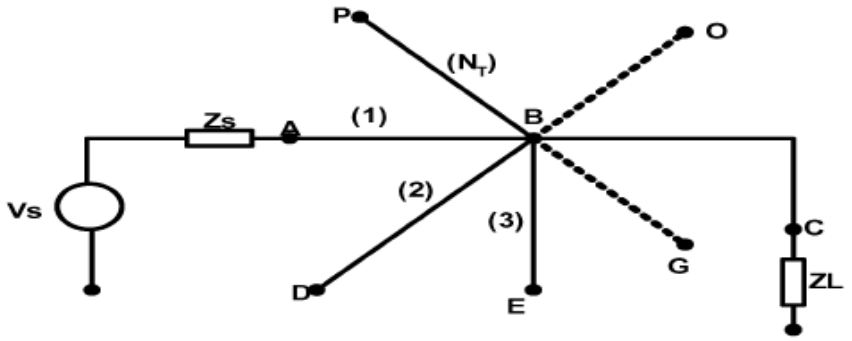

Figure 2.3: Multiple branches at a single node [49]

$$V_m(f) = H_m(f).\Big(\frac{Z_{Ln}}{Z_{Ln} + Z_s}\Big)V_s \tag{2.8}$$

where N_T is the total number of branches connected to the node B and terminated in any arbitrary node, m is any referenced terminated load, M is the number of reflections (with total L number of reflections), T_{LM} is the transmission factor at the referenced load m, $H_{mn}(f)$ is the transfer function between the line and the reflected load and α_{mn} is the signal contribution factor and is given by [48, 49]:

$$\alpha_{mn} = P_{Ln}^{M-1}\rho_{nm}^{M-1}e^{-\gamma_n(2(M-1)l_n)} \tag{2.9}$$

where:

$$P_{Ln} = \begin{cases} \rho_s & n = 1(\text{source}) \\ \rho_{Ln} & \text{otherwise} \end{cases} \tag{2.10}$$

and γ_n is the propagation constant of line n, with a length l_n and ρ_{mn} is the reflection factor at node B between line n and referenced load m. For a power line network with more that one node as shown in Fig. (2.4),the resultant transfer function will be given by [48, 49]:

$$H_{mM_T}(f) = \prod_{d=1}^{M_T}\sum_{M=1}^{L}\sum_{n=1}^{N_T} T_{Lmd}\alpha_{mnd}H_{mnd}(f), \qquad n \neq m \tag{2.11}$$

where all the parameters used have the same meaning as those of (2.7) but with reference node d, M_T is the total number of distributed nodes and:

$$\alpha_{mnd} = P_{Lnd}^{M-1}\rho_{nmd}^{M-1}e^{-\gamma_{nd}(2(M-1)l_{nd})} \tag{2.12}$$

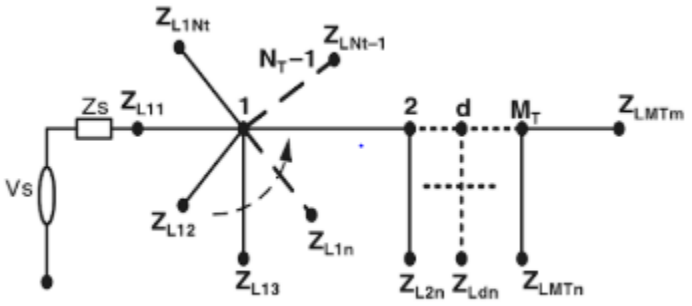

Figure 2.4: Power line network with distributed branches [49]

$$P_{Lnd} = \begin{cases} \rho_s & d = n = 1(\text{source}) \\ \rho_{Lnd} & \text{otherwise} \end{cases} \tag{2.13}$$

$$V_{mM_T}(f) = H_{mM_T}(f).\Big(\frac{Z_{Ldn}}{Z_{Ldn} + Z_s}\Big)V_s \tag{2.14}$$

2.2.4 Philipps' Series Resonant Circuit (SRC) Model

This model describes the power line channel as a cascade of decoupled series resonance circuits [47]. This is based on the fact that many appliances connected to PLC network do posses a feeding line composed of resistive and inductive portions and incorporate anti-interference capacitors at their inputs. Moreover, from impedance measurements, electrical loads can be described by one or a few series resonant circuits made up of resistance R, inductance L and capacitor C. Figure 2.5 shows a series resonant circuit connected to a line with impedance Z. The impedance of the resonant circuit depends on frequency is shown in Figure 2.5, and can be given by:

$$Z_s(f) = R + \jmath 2\pi f l + \frac{1}{\jmath 2\pi f C} \tag{2.15}$$

At resonance, the real part of $Z_s(f)$ will be equal to R while the imaginary part will be equal to zero since X_l and X_c will be equal. The resonance frequency f_{res} is given by:

$$f_{res} = \frac{1}{2\pi\sqrt{LC}} \tag{2.16}$$

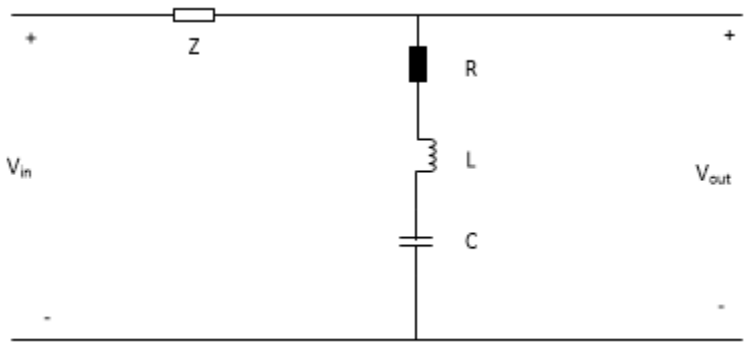

Figure 2.5: Series resonant circuit

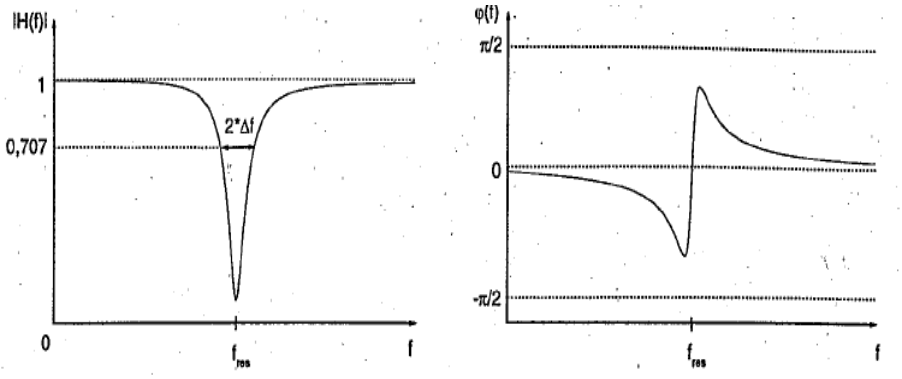

Figure 2.6: Amplitude and phase characteristic of a series resonant circuit [47]

The transfer function of the circuit is thus given by [47]

$$H(f) = \frac{Z_s(f)}{Z_s(f) + Z} \tag{2.17}$$

At frequencies below and above the resonant frequency, the transfer function is approximately 1 as shown in Figure 2.6.
A notch is seen to be at resonant frequency and its depth depends on resistance R and impedance Z. The width of the notch defines the quality factor Q of the resonant circuit and can be given by [47]:

$$Q = \frac{f_o}{2\Delta f} \tag{2.18}$$

where f_o is the resonant frequency and Δf is the 3-dB bandwidth. Thus, the lower the Q the wider the notch and vice versa. For N cascaded resonant circuits, the overall transfer function can be obtained as:

$$H(f) = \prod_{v=1}^{N} H_i(f) \tag{2.19}$$

where $H_i(f)$ is the transfer function of each resonant circuit.

2.2.5 Parallel Resonant Circuit Model

This model describes the PLC channel as a cascade of parallel resonant circuits [51, 52] and is adapted from [47]. It also describes electrical loads as a composition of resistance R, inductance L, and capacitance C. In this model the correlation between the notch positions and the branch parameters was obtained through measurement. The input impedance characteristics around a resonant wavelength λ_o for open-circuited and short-circuited transmission line were analyzed using the transmission line theory. For both cases, the transmission line behave like a parallel resonant circuit whereby for the open-circuit case cable length is in even multiples of $\frac{\lambda_o}{2}$ and for the short-circuit case the cable length is in even multiples of $\frac{\lambda_o}{4}$. The transfer function for each resonant circuit is given by [51, 52]

$$H(f) = \frac{Z_o}{Z_o + Z_p(f)} \tag{2.20}$$

where Z_o is the characteristic impedance of the circuit and $Z_p(f)$ is the frequency dependent input impedance of the parallel resonant circuit give by:

$$Z_p(f) = \left(\frac{1}{R} + \frac{1}{\jmath\omega L} + \jmath\omega C \right)^{-1} \tag{2.21}$$

If there are N cascaded parallel resonant circuits in the network,where each circuit has a transfer function $H_p(f)$, then overall transfer function will be given by:

$$H(f) = A \prod_{v=1}^{N} H_p(f) \tag{2.22}$$

The parameters for the parallel RLC are summarised in Table 2.1 where ω_o is the angular resonant frequency and α is the attenuation constant of the line. A is a function of frequency and length l, and is defined as the direct path loss factor from the transmitter to the receiver and is given as [43, 52]

$$A(f, l) = e^{-\alpha(f)l} \tag{2.23}$$

Table 2.1: Parallel Resonance RLC parameters

Resonance	Open-circuit ($\frac{\lambda_o}{2}$)	Short-circuit ($\frac{\lambda_o}{4}$)
R	$\frac{2Z_o}{\alpha\lambda_o}$	$\frac{4Z_o}{\alpha\lambda_o}$
L	$\frac{2Z_o}{\pi\omega_o}$	$\frac{4Z_o}{\pi\omega_o}$
C	$\frac{\pi}{2\omega_o Z_o}$	$\frac{\pi}{4\omega_o Z_o}$

2.3 The Impact of the PLC Impedance on the PLC Channel Modeling

The transfer functions of the various models discussed that were developed using the deterministic approach are seen to depend on the impedance of the power line network. The same case applies for the Meng et al. [44] and Esimilan et al. [54] models. The echo model [47] and the multipath model [43] developed through the top-down approach also consider signal reflections caused by points of impedance discontinuities. Thus, if the behavior of the PLC network impedance can be modeled, then the characteristics of the power line network can be known and hence the improvement of the channel transfer function. This is further discussed in chapter 4 where the input impedance of the PLC network is modeled, characterised and profiled. For the models developed using the deterministic approach, the transmission line theory is used to derive the parameters of the channel. This is observed to be true in the bottom-up approach employed for the multipath model as represented in [55], and also in obtaining the impedance parameters in the Meng et al. [44], Esimilan et al. [54], Zwane and Afullo model [50], and the parallel resonant approach in [51, 52]. Therefore, the knowledge of the transmission line is fundamental for modeling of the power line channel.

2.4 Transmission Line Theory

PLC utilises the transmission line as its media of transfer of the high frequency communication signals. Thus, in the development of the power line channel models using the bottom-up approach, a detailed knowledge of the characteristics of the transmission line is required. The transmission line theory is similar to circuit theory with the major difference being the electrical size. While transmission lines may be a considerable fraction of a wavelength or wavelengths long, circuit analysis assumes that the physical dimensions of the network are much smaller than the electrical length and hence the ordinary circuit analysis deals with lumped elements while the transmission line is a distributed electrical network. In PLC, communication signals propagate through the transmission line governed by transverse electromagnetic wave propagation and is normally represented as a two-wire line.

For an infinitesimal length Δz, the transmission line can be modeled as a lumped-element circuit with per-unit-length parameters R, L, C and G which represent the series

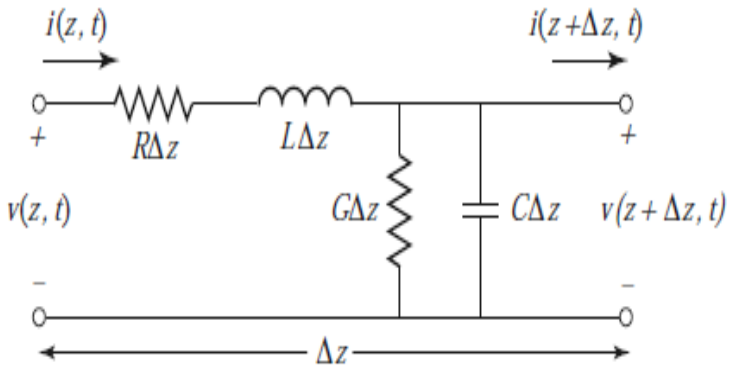

Figure 2.7: Lumped equivalent circuit of the transmission line [56]

resistance for both conductors in Ω/m, series inductance for both conductors in H/m, shunt capacitance in F/m and shunt conductance in S/m respectively as shown in Figure 2.7. Thus for a transmission line of a finite length, its elements can be determined as a cascade of the lumped elements. The instantaneous voltage and current at a location z of the transmission line are represented by $v(z,t)$ and $i(z,t)$ respectively, and at location Δz, the instantaneous voltage and current are given by $V(z+\Delta z)$ and $I(z+\Delta z)$ respectively. By applying Kirchhoff's voltage law and Kirchhoff's current law we obtain [56, 57]:

$$v(z,t) = R\Delta z i(z,t) + L\Delta z \frac{\partial i(z,t)}{\partial t} + v(z+\Delta z,t) \tag{2.24}$$

$$i(z,t) = G\Delta z v(z+\Delta z,t) + C\Delta z \frac{\partial v(z+\Delta z,t)}{\partial t} + i(z+\Delta z,t) \tag{2.25}$$

Taking the limit as $\Delta z \to 0$ in (2.24) and (2.25) and dividing both equations by Δz we obtain the Telegraphers equations given by [56, 57]:

$$-\frac{\partial v(z,t)}{\partial z} = Ri(z,t) + L\frac{\partial i(z,t)}{\partial t} \tag{2.26}$$

$$-\frac{\partial i(z,t)}{\partial z} = Gv(z,t) + C\frac{\partial v(z,t)}{\partial t} \tag{2.27}$$

Equations (2.26)and (2.27) can further be simplified to (2.28) and (2.29), respectively, when considering sinuisodal steady-state conditions with cosine -based phasors as:

$$-\frac{dV(z)}{dz} = I(z)(R + \jmath\omega L) \tag{2.28}$$

$$-\frac{dI(z)}{dz} = V(z)(G + \jmath\omega C) \tag{2.29}$$

The wave equations for V(z) and I(z) can then be determined by solving equations (2.28) and (2.29) as:

$$\frac{d^2V(z)}{dz^2} - \gamma^2 V(z) = 0 \tag{2.30}$$

$$\frac{d^2I(z)}{dz^2} - \gamma^2 I(z) = 0 \tag{2.31}$$

where γ is the complex propagation constant of the line and is given by [56, 57]:

$$\gamma = \alpha + \jmath\beta = \sqrt{(R + \jmath\omega L)(G + \jmath\omega C)} \tag{2.32}$$

where α is the attenuation constant and β is the phase constant. The solutions for the traveling waves in (2.30) and (2.31) are then determined as:

$$V(z) = V_o^+ e^{-\gamma z} + V_o^- e^{\gamma z} \tag{2.33}$$

$$I(z) = I_o^+ e^{-\gamma z} + I_o^- e^{\gamma z} \tag{2.34}$$

where V_o^+, V_o^-, I_o^+ and I_o^- are the amplitudes of the waves, $e^{\gamma z}$ and $e^{-\gamma z}$ represent the wave propagation in the $-z$ direction and $+z$ direction, respectively. At any given point in an infinitely long transmission line, the ratio of voltage to current at that point is equal and referred to as the characteristic impedance Z_o and is given by :

$$Z_o = \frac{V_1}{I_1} = \frac{V_2}{I_2} = ... = \frac{V_n}{I_n} \tag{2.35}$$

The characteristic impedance of the transmission line is very important in the modeling of PLC channel as it determines the transmission and reflection factors at points of discontinuity. It can also be found by applying (2.28) to (2.30) to determine the current on the line:

$$I(z) = \frac{\gamma V(z)}{R + \jmath\omega L} \tag{2.36}$$

The characteristic impedance can then be determined as [56, 57]:

$$Z_o = \frac{V(Z)}{I(z)} = \frac{R + \jmath\omega L}{\gamma} \tag{2.37}$$

$$Z_o = \sqrt{\frac{R + \jmath\omega L}{G + \jmath\omega C}} \tag{2.38}$$

2.4.1 Input Impedance of a Terminated Transmission Line

As mentioned earlier, various loads are plugged in and out of the power line network via the socket outlets leading to the variation in the input impedance of the power line network. Thus, having analyzed the lumped-circuit parameters of the transmission line, it is also important to analyze the input impedance of a transmission line terminated by a load Z_l, that is not equal to the characteristic impedance Z_o located at a distance l, from the source as shown in Figure 2.8.

The ratio of the voltage to current at the load will be equal to Z_l and hence the amplitude of the reflected wave must be excited enough to satisfy this condition. The total voltage of the line will thus be given by [56, 58]:

$$V(z) = V_o^+ e^{-\gamma z} + V_o^- e^{\gamma z} \tag{2.39}$$

where V_o^+ and V_o^- are the incident voltage and reflected voltage respectively. Since Z_o is the ratio of voltage to current of a traveling wave, the total current on the line can be described by:

$$I(z) = \frac{V_o^+}{Z_o} e^{-\gamma z} - \frac{V_o^-}{Z_o} e^{\gamma z} \tag{2.40}$$

At $z = 0$, the input impedance of the transmission line can be determined as [56, 58]:

$$Z_{in} = \frac{V(z=0)}{I(z=0)} = \frac{V_o^+ + V_o^-}{V_o^+ - V_o^-} Z_o \tag{2.41}$$

Dividing (4.14) by the incident voltage, the input impedance becomes:

$$Z_{in} = Z_o \frac{1 + \Gamma_o}{1 - \Gamma_o} \tag{2.42}$$

where Γ_o is the input reflection coefficient. At $z = l$, the total voltage and current are related to the load impedance as [56, 58]:

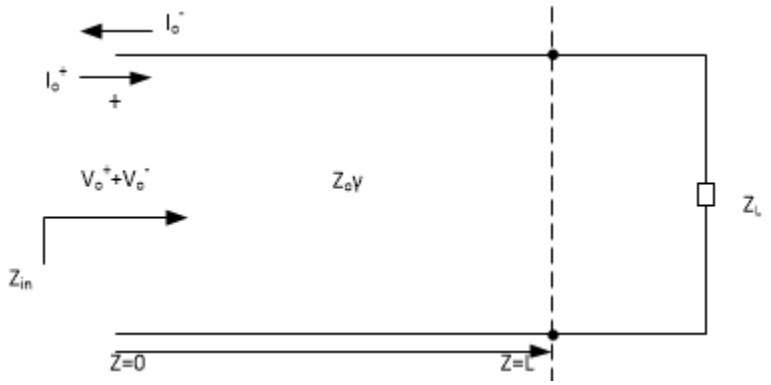

Figure 2.8: Transmission line terminated by a load

$$Z_l = \frac{V(z=l)}{I(z=l)} = Z_o \frac{V_o^+ e^{-\gamma l} + V_o^- e^{\gamma l}}{V_o^+ e^{-\gamma l} - V_o^- e^{\gamma l}} \tag{2.43}$$

Equation (2.43) can further be simplified as:

$$Z_l = Z_o \frac{e^{-\gamma l} + \Gamma_o e^{\gamma l}}{e^{-\gamma l} - \Gamma_o e^{\gamma l}} \tag{2.44}$$

Substituting (2.44) into (2.42) the input impedance of the transmission can be re-written as [56, 58]:

$$Z_{in} = Z_o \frac{Z_l + Z_o \tanh \gamma l}{Z_o + Z_l \tanh \gamma l} \tag{2.45}$$

2.4.2 Two-conductor Transmission Line

In the modeling of the PLC channel, the two-conductor approach is much simpler to implement and therefore is often preferred for approximation of the channel transfer function and the input impedance of the power line. These models utilize either the transmission matrix or the scattering matrix approach for the transfer function and impedance and admittance matrices for the power line impedance. The impedance matrix is useful in the design of passive components such as filters and couplers in the power line channel most of which utilize the two-port T and Pi-networks.

A two-port network with a voltage V_1 and current I_1 at port-1 and a voltage V_2 and current V_2 at port port-2 is as shown in Figure 2.9. From superposition theorem, the impedance matrix can be represented as [56, 57]:

$$\begin{bmatrix} V_1 \\ V_2 \end{bmatrix} = \begin{bmatrix} Z_{11} & Z_{12} \\ Z_{21} & Z_{22} \end{bmatrix} \begin{bmatrix} I_1 \\ I_2 \end{bmatrix} \tag{2.46}$$

The admittance matrix can then be obtained by finding the inverse of the impedance matrix. The scattering parameters provide a complete description of the power line network as seen by the ports of the communication devices. Unlike the impedance matrix that relate to the port voltages and currents, the scattering parameters relates to incident and reflected waves. Thus if a_1 and b_1 are the incident waves and reflected waves for port-1 and port-2 respectively and a_2 and b_2 are the incident and reflected waves for port-2 respectively as shown in Fig. 2.10, then mathematically [56, 57],

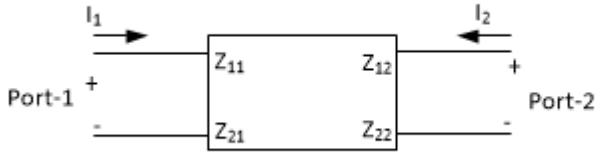

Figure 2.9: Impedance matrix of a two-port network

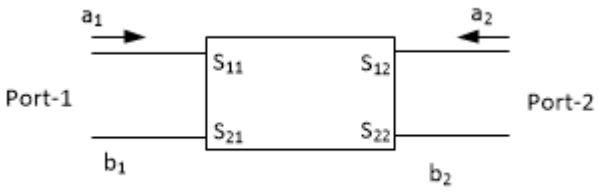

Figure 2.10: Two-port network scattering matrix

$$b_1 = S_{11}a_1 + S_{12}a_2 \tag{2.47}$$

$$b_2 = S_{21}a_1 + S_{22}a_2 \tag{2.48}$$

and the scattering matrix notation will be represented as [56, 57]:

$$\begin{bmatrix} b_1 \\ b_2 \end{bmatrix} = \begin{bmatrix} S_{11} & S_{12} \\ S_{21} & S_{22} \end{bmatrix} \begin{bmatrix} a_1 \\ a_2 \end{bmatrix} \tag{2.49}$$

It is then possible to convert the scattering parameters to ABCD parameters as described in [56, 57].

2.5 Impedance Matching

The output impedance of the transmitter and the receiver in a PLC system are generally designed to a fixed value of 50 Ω – 75 Ω [59]. However, the power line impedance varies greatly with the time and location resulting in impedance mismatch between the communication equipment and the power line. This leads to high signal reflection that reduces the power delivered to the receiver as well as deterioration in signal quality [40, 60, 61]. Therefore, impedance matching is of paramount importance in PLC. The impedance matching networks are employed both at the transmitter and at the receiver together with the coupling interface and therefore act as a boundary between the sensitive communication equipment and the harmful power line voltages and currents [62]. The block diagram for a power line network with the matching circuits is as shown in Figure 2.11.

There are three main approaches to the design of impedance matching networks and they include complex conjugate matching, equal impedance matching and voltage maximization matching. In complex conjugate matching, the source impedance is designed to minimize the power reflection coefficient and is the the most commonly used method for maximum signal transfer in transmission lines [63]. The equal impedance matching approach is based on minimizing the reflected wave voltage from the power line to the generator. The voltage maximization matching on the other hand, is based on maximizing the voltage amplitude at the input port. This is done by choosing the real part of the source impedance to be zero and while the imaginary part of the source impedance is opposite that of the load.

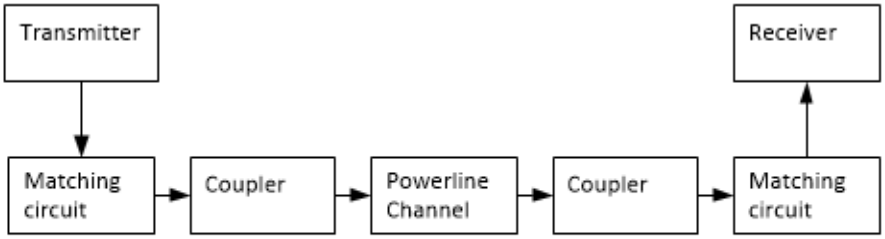

Figure 2.11: Block diagram of the power line network

Impedance matching in the PLC network can also be achieved through impedance transformation networks that include transmission line stubs [64] and the use of lumped elements employed in [62, 65, 66] . In transmission line stub matching technique, the transmission feed line is connected in either series or parallel to an open-circuited or short-circuited length of transmission line (stub) at a certain distance from the load, as shown in Figures 2.12 and 2.13. The reactance is tuned by adjusting the length of the series-stub d, such that the impedance Z, looking into the line at a distance d from the load is opposite that of the load, that is, if the load impedance is $Z_o + \jmath X$ then the stub reactance is chosen as $-\jmath X$. For the parallel-stub, the distance d is chosen such that the admittance Y, seen looking into the line from the load is $Y_o + \jmath B$ while the stub susceptance is $-\jmath B$ resulting in a matched condition. Impedance matching using transmission line stub however, may not be feasible in certain high frequencies due to the size. The wavelength for a 100 MHz signal for example, is 3 m and thus may not be practical for implementation on a printed circuit board [57]. Therefore, for broadband frequency applications in PLC , the lumped elements are used. The lumped element matching technique uses reactive elements to match the transmission line to an arbitrary load impedance. The values of the reactive elements are chosen according to the load impedance and may either be inductors or capacitors arranged to form L-sections and utilizes the conjugate matching approach. Alternative matching techniques have also been proposed in [67], where matching is

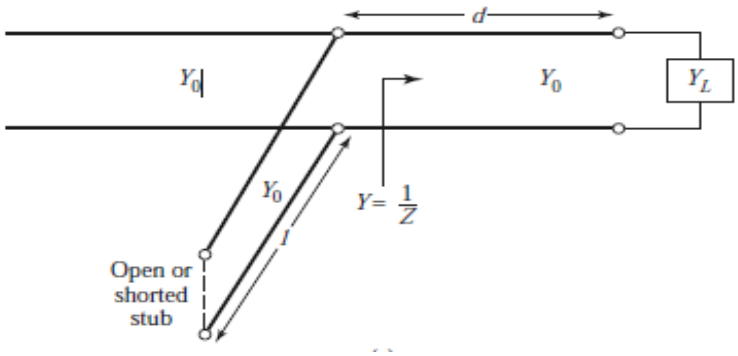

Figure 2.12: Parallel Stub [56]

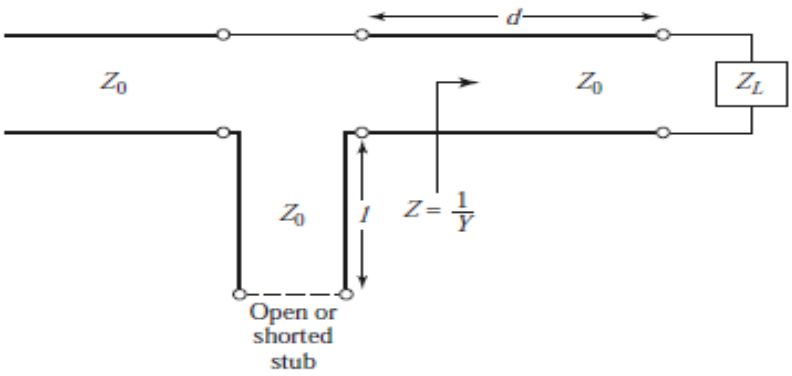

Figure 2.13: Series Stub [56]

accomplished by varying the inductance by changing the tap of the coupling transformer. In [68], a capacitor bank comprising of a number of high voltage blocking capacitors in parallel to match the inductive reactance of the channel is proposed. The use of voltage controlled general impedance converter where operational amplifiers, resistors and capacitors are used to produce impedance that matches that of the transmission line is employed in [69]. These alternative techniques are much more suited for narrow-band PLC applications.

2.6 Chapter Summary

In this chapter, the parametric and deterministic approaches of modeling the power line channel have been described whereby the former utilizes measurements to derive its parameters for the proposed model while in the latter detailed knowledge of the charactyeristics of the network and its physical structure is requiered to model the power line channel. From the analysis, the channel transfer function is seen to depend on the impedance of the power line network. The two-conductor transmission line has also been reviewed where the impedance and scattering parameters used by the vector network analyzer to display the channel characteristics are also discussed. The improvement of the power line impedance through matching circuits has has been reviewed where conjugate matching is seen to be the commonly used approach. Transmission line stubs are seen to have reactive properties depending on their length which can the be used to match the reactive part of the transmission line impedance.

Chapter 3

DETERMINATION OF THE INTRINSIC POWER LINE PARAMETERS

3.1 Introduction

In chapter 2, various modelling techniques of the PLC channel have been discussed. The various models have been classified under two categories; the top-down and the bottom-up approaches. The extraction of the line parameters gives a background knowledge of the PLC channel and thus considered of major importance. In this chapter, two methods of line parameter extraction have been considered. As shall be seen later in chapter 4, the impedance modeling procedure adopts a bottom-up strategy, within which the cable primary parameters are required. Firstly, the power line cables are treated as two-conductor transmission lines and the theory of transverse electromagnetic (TEM) propagation applied. This allows for a theoretical extraction of the characteristic impedance, Z_o, propagation constant γ, and distributed primary parameters in the form of resistance per unit length $R\prime$, inductance per unit length $L\prime$, conductance per unit length $G\prime$, and capacitance per unit length $C\prime$. Secondly, the same parameters are obtained through measurements by measuring the cable's S-parameters. A comparison between the results obtained through the two approaches is made to emphasize the importance of cable variety as is common within the power delivery fraternity.

3.2 Theoretical Extraction of Line Parameters

In this method of extracting the line parameters, the $R\prime$, $L\prime$, $G\prime$ and $C\prime$ are first derived by electromagnetic field analysis of the transmission line taking into consideration the dielectric characteristics of the insulating material, the conducting material as well as the cross-sectional dimensions of the cable. Most indoor power line cable consists of three conductors as shown in Figure 3.1. The distributed parameters are used to determine the characteristic impedance Z_o, and the propagation constant γ, of the line as [56, 57]:

$$Z_o = \sqrt{\frac{R\prime + \jmath\omega L\prime}{G\prime + \jmath\omega C\prime}} \tag{3.1}$$

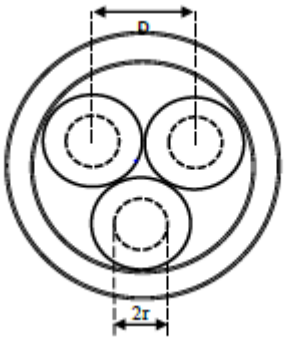

Figure 3.1: Cross-section area of a cable

and:

$$\gamma = \sqrt{(R\prime + \jmath\omega L\prime)(G\prime + \jmath\omega C\prime)} \tag{3.2}$$

3.2.1 Per Unit Resistance

The resistance of a power line cable is a result of the finite nature of the conductivity of the individual conductors. The resistance increases with increase in frequency as self-inductance within the conductor causes more current to flow near the outer surface of the conductor due to skin effect. The per unit length resistance is thus given as [70]:

$$R\prime = \sqrt{\frac{2f\mu_r\mu_o}{\pi r^2\sigma_c}}\left(\frac{\frac{D}{2r}}{\sqrt{(\frac{D}{2r})^2 - 1}}\right) \tag{3.3}$$

where f is the frequency of the wave, σ_c is the electric conductivity of the material ($5.58 \times 10^7\ S/m$), r is the conductor radius, D is the distance of separation between conductors, μ_r is the relative magnetic permeability of the dielectric material and μ_o is the magnetic permeability in free space given by $4\pi \times 10^{-7} H/m$.

3.2.2 Per Unit Inductance

For a two-conductor transmission line, the inductance is due to the skin-effect L_{int} (internal inductance) and that produced by the fields outside the conductor L_{ext} (external inductance). The internal inductance decreases with increase in frequency and as such at high frequencies the internal inductance is very small. The total inductance per unit length $L\prime$ is thus given by [71]:

$$L\prime = L_{in} + L_{ex} = \frac{R\prime}{2\pi f} + \frac{\mu_r\mu_o}{\pi}\cosh^{-1}\left(\frac{D}{2r}\right) \tag{3.4}$$

where f is the frequency of the wave, r is the conductor radius, D is the distance of separation between conductors, μ_r is the relative magnetic permeability of the dielectric

material and μ_o is the magnetic magnetic permeability in free space given by $4\pi \times 10^{-7} H/m$.

3.2.3 Per Unit Capacitance

Due to the close proximity of the conductors, there is a leakage capacitance between the conductors through the cable's dielectric material that is proportional to the electric field established by a potential difference between the two conductors given by [72]:

$$C\prime = \frac{\pi \epsilon_r \epsilon_o}{\cosh^{-1}\left(\frac{D}{2r}\right)} \tag{3.5}$$

where r is the radius of the conductor, D is the distance of separation between conductors, ϵ_r is the relative dielectric constant and ϵ_o is the electric permittivity given by $8.85 \times 10^{-12}\ F/m$.

3.2.4 Per Unit Conductance

The conductance in the cables is due to the dielectric loss of the insulating material between the conductors. When the medium is considered homogeneous, the conductance per unit length is determined as [73]:

$$G\prime = 2\pi f C\prime \tan\delta \tag{3.6}$$

$$\delta = \frac{1}{\sqrt{2\pi\sigma_c\mu_c}} \tag{3.7}$$

where f is the wave frequency and $\tan\delta$ is the dissipation factor. The current distribution on the conductor cross-sectional area is described by the skin depth σ, determined as [74]:

$$\sigma = \frac{1}{\sqrt{2\pi f\sigma_c\mu_c}} \tag{3.8}$$

where μ_c is the relative permeability of the conductor and σ_c the conductivity of the material given by $5.58 \times 10^7 S/m$.

3.3 Extraction of Line Parameters Through Measurements

In this method of line parameter extraction, the characteristic impedance and the propagation constant of the line are first determined from the vector network analyzer S_{11} measurements and then the $R\prime$, $L\prime$, $C\prime$ and $G\prime$ are determined from the characteristic impedance and the propagation constant. The S_{11} parameter is ratio of the reflected to the incident wave at port-1 of the analyser and gives an estimate of the normalized input reflection coefficient which is such that [56, 57]:

$$\Gamma_{in} = S_{11}\angle\phi \tag{3.9}$$

Also,

$$\Gamma_{in} = \frac{Z_{in} - Z_o}{Z_{in} + Z_o} \tag{3.10}$$

where Γ_{in} is the measured complex reflection coefficient and Z_o is the reference port impedance of the vector network analyzer. From (3.10), the input impedance of the line can be determined as:

$$Z_{in} = Z_o \frac{1 + \Gamma_{in}}{1 - \Gamma_{in}} \tag{3.11}$$

The input admittance can then be given by:

$$Y_{in} = \frac{1}{Z_{in}} \tag{3.12}$$

In order to determine the propagation constant γ, and the characteristic impedance Z_o, of the line, we consider a transmission line terminated by a load Z_l at a distance l, from the generator end as shown in Figure 3.2. From the transmission line theory, the input impedance Z_{in} of the line will be given by [56, 57]:

$$Z_{in} = Z_o \frac{Z_l + Z_o \tanh \gamma l}{Z_o + Z_l \tanh \gamma l} \tag{3.13}$$

For $Z_l = 0$, implying a short-circuit, the input impedance Z_{sc}, is determined as:

$$Z_{sc} = Z_o \tanh \gamma l \tag{3.14}$$

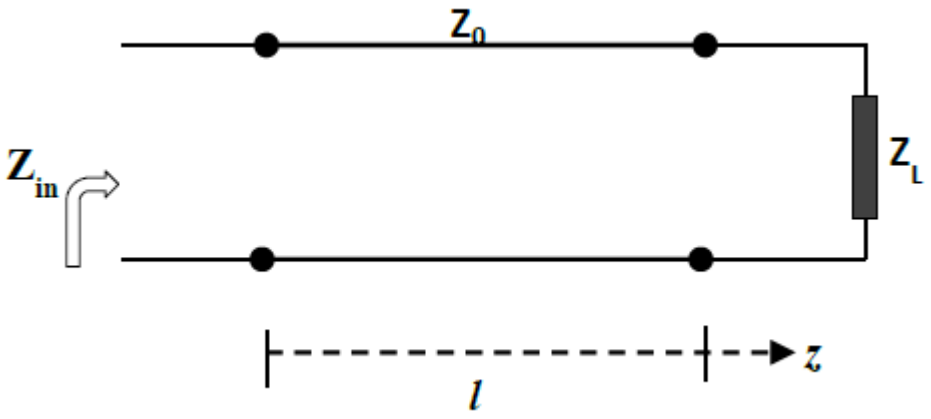

Figure 3.2: Determination of Reflection Coefficient

whereas, for $Z_l = \infty$, implying an open-circuit, the input impedance Z_{oc} is given by:

$$Z_{oc} = Z_o \coth \gamma l \tag{3.15}$$

Thus, the characteristic impedance can be determined from (3.14) and (3.15) as [56, 57]:

$$Z_o = \sqrt{Z_{sc} Z_{oc}} \tag{3.16}$$

whereas, the propagation constant is determined as [56, 57]:

$$\gamma = \frac{1}{l} \tanh^{-1} \sqrt{\frac{Z_{sc}}{Z_{oc}}} \tag{3.17}$$

The distributed parameters of the transmission line are then obtained from the Z_0 and γ as [75]:

$$R\prime = \Re(\gamma . Z_o) \tag{3.18}$$

$$G\prime = \Re\left(\frac{\gamma}{Z_o}\right) \tag{3.19}$$

$$L\prime = \Im\left(\frac{\gamma . Z_o}{\omega}\right) \tag{3.20}$$

$$C\prime = \Im\left(\frac{\gamma . \omega}{Z_o}\right) \tag{3.21}$$

where $\Re(.)$ and $\Im(.)$ represent the real and imaginary parts, respectively, and ω is the angular frequency.
The distributed parameters can also be determined from the input impedance considering a short-circuit and an open-circuit load conditions. In this approach, the parameters $R\prime$ and $L\prime$ are obtained from Z_{sc} and $G\prime$ and $C\prime$ are obtained from Z_{oc} as follows [72]:

- Resistance and Inductance: These parameters are measured by terminating the end of the cable with a short-circuit to obtain the input impedance Z_{sc}. This will then establish a connection through the series elements $R\prime$ and $L\prime$ as shown in Figure 3.3. The real and imaginary parts of Z_{sc} represent the resistance and inductance of the line, respectively.

- Conductance and capacitance: These parameters are measured by terminating the end of the cable with an open-circuit to obtain the input impedance Z_{oc}. This will effectively establish a connection through the shunt elements $G\prime$and $C\prime$ as shown in Figure 3.4. The real and imaginary parts of Z_{oc} represent the conductance and capacitance of the line, respectively.

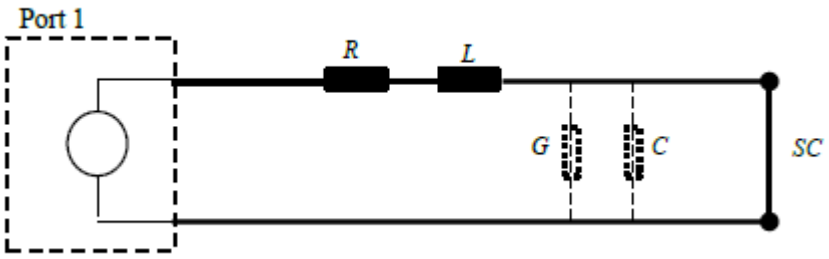

Figure 3.3: Measurement with short termination [72]

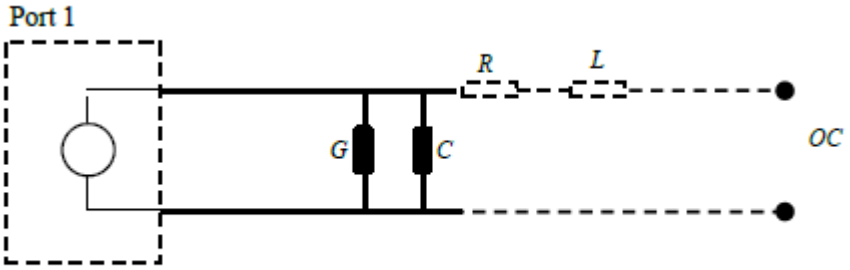

Figure 3.4: Measurement with open termination [72]

3.4 Measurement Equipment and Set-up

The TR5048 vector network analyzer was used to obtain the S_{11} parameters measurements for Cu 3×2.5 mm^2 Cabtyre flexible PVC power line cable used by the local utility for the test network. The main objective of the measurements is to obtain the transmission line parameters as well as compare them with the theoretical values. In order to enhance the accuracy of the measurements, a full one-port calibration was performed since the measurement required were the S_{11} parameters. In this method of calibration, the SHORT, OPEN and LOAD standards are used to calibrate port-1, eliminating the frequency-dependent attenuation and phase offset in the measurement circuit. Thereafter, the measurement was carried out for the set-ups shown in Figures 3.3 and 3.4. Measurements were done for a frequency range of 1–30 MHz using a 99 m long cable.

3.5 Measurement Results

The normalized S_{11} parameter measurement results for the short-circuit and open circuit terminated cables obtained directly from the vector network analyzer are as shown in Figures 3.5 and 3.6 respectively.

The normalized reflection measurement results are then used to determine the input impedances for the open-circuit and short-circuit terminations. The real and the imaginary

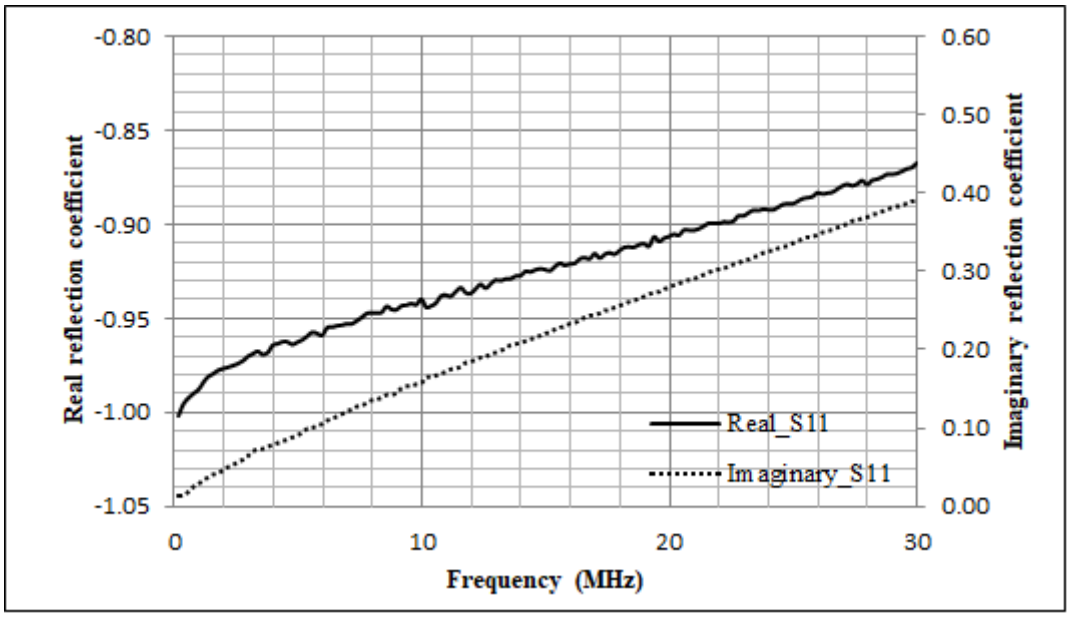

Figure 3.5: Normalized S_{11} parameters for short-circuit cable termination

parts of the Z_{sc} and Z_{oc} are shown in Figures 3.7 and 3.8 respectively. There are oscillations in both cases at lower frequencies and this is due to cable resonance at those frequencies. As the frequency increases, the reflected wave from the point of mismatch is attenuated almost completely and hence the peaks are also diminished. The distributed parameters $R\prime$, L$\prime$, $G\prime$ and $C\prime$ are then obtained from the Z_{sc} and the Z_{oc} measurement results through the procedure explained in section 3.3 and are shown in Figures 3.9 through 3.12 respectively. The measurement results for the distributed line parameters are compared to the theoretical values obtained from the model calculations in section 3.3 where they show a good agreement except for the deviations due to dielectric materials, observed with the conductance and resistance. The measurement and the theoretical results for the characteristic impedance are shown in Figure 3.13. The values used for the dielectric characteristics were obtained from [76] where experiments were performed in the research study.

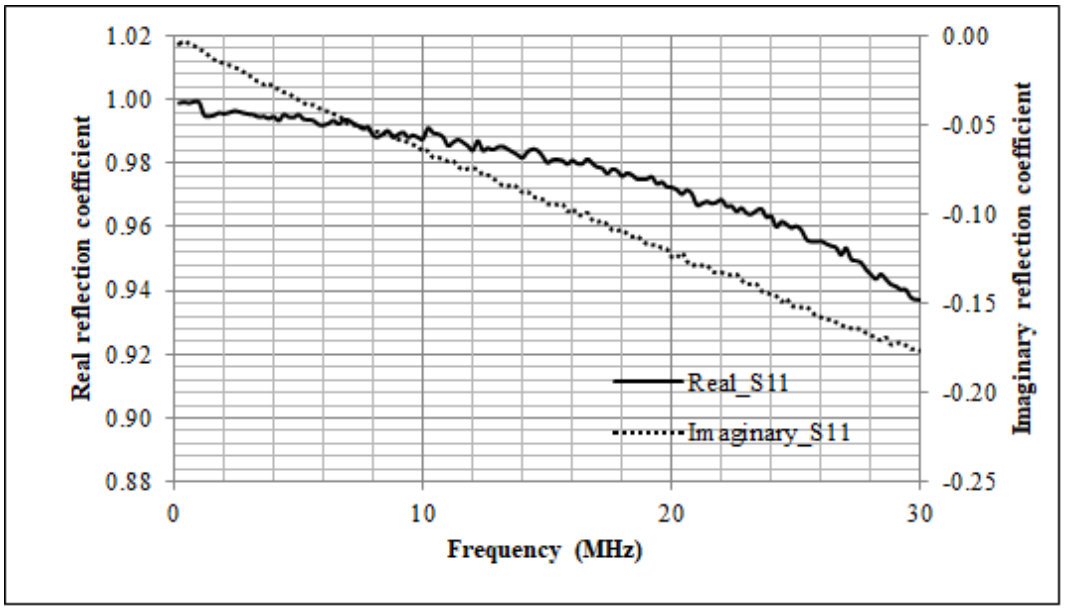

Figure 3.6: Normalized S_{11} parameters for open-circuit cable termination

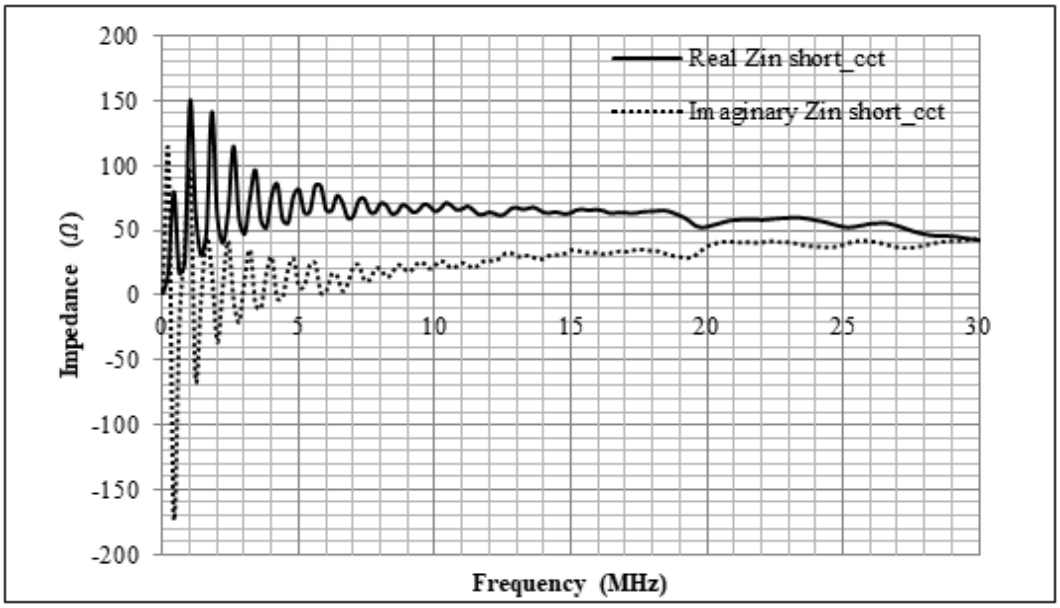

Figure 3.7: Input impedance for short-circuit cable termination

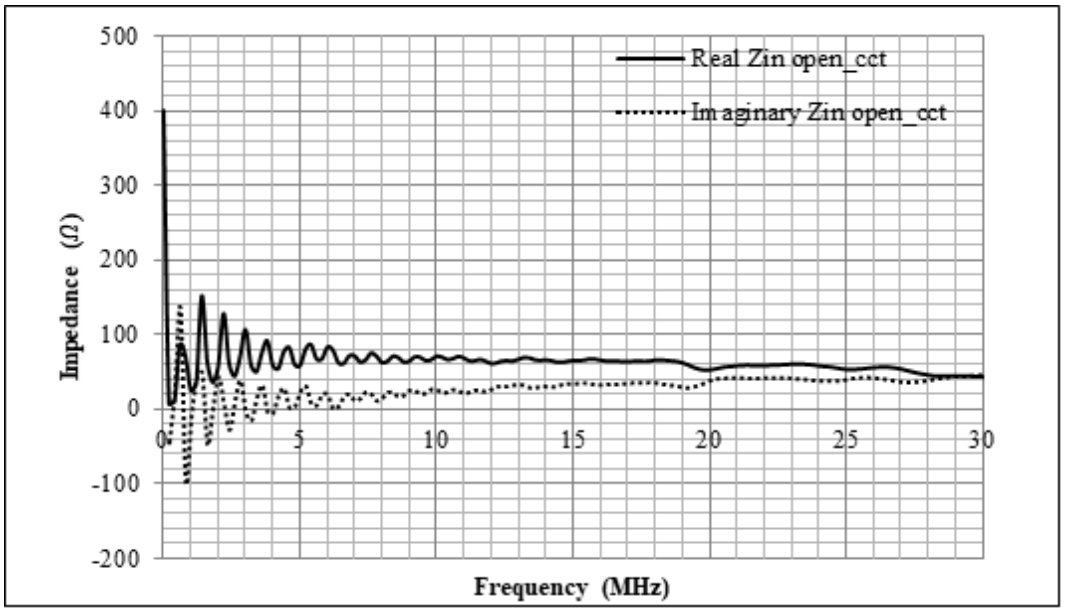

Figure 3.8: Input impedance for open-circuit cable termination

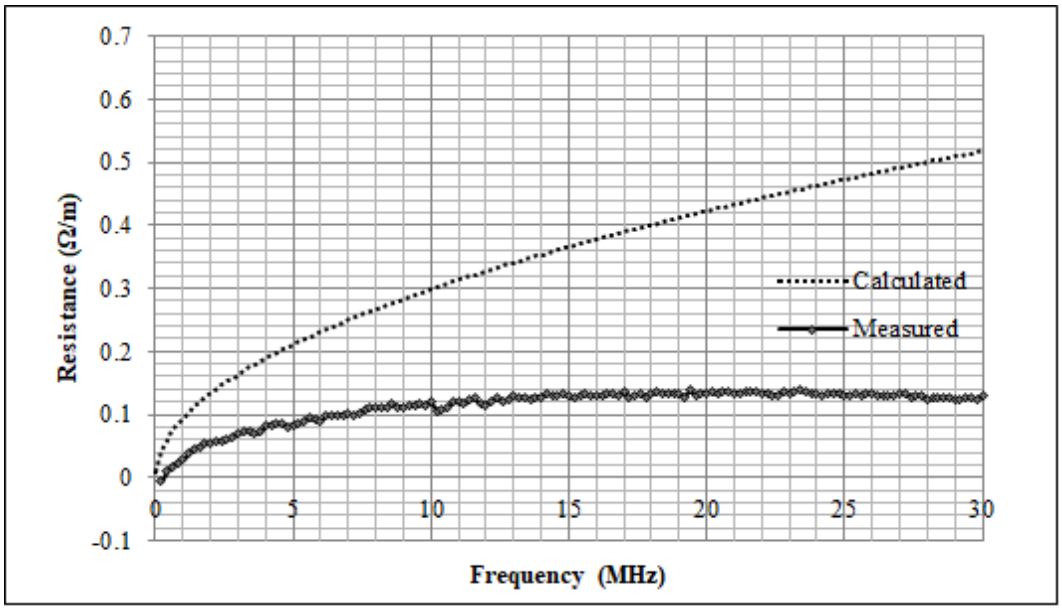

Figure 3.9: Resistance per unit length

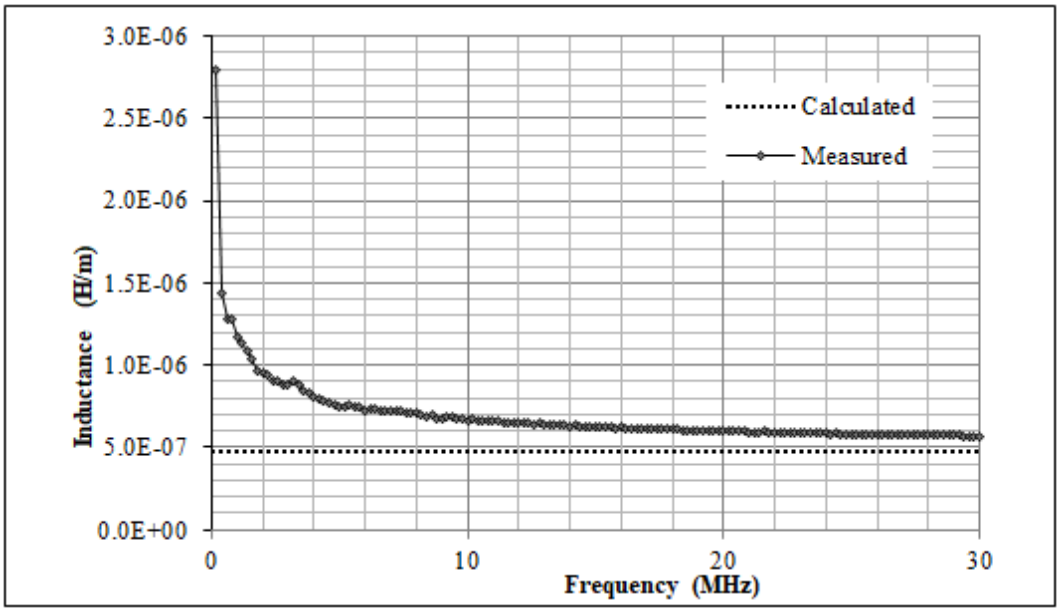

Figure 3.10: Inductance per unit length

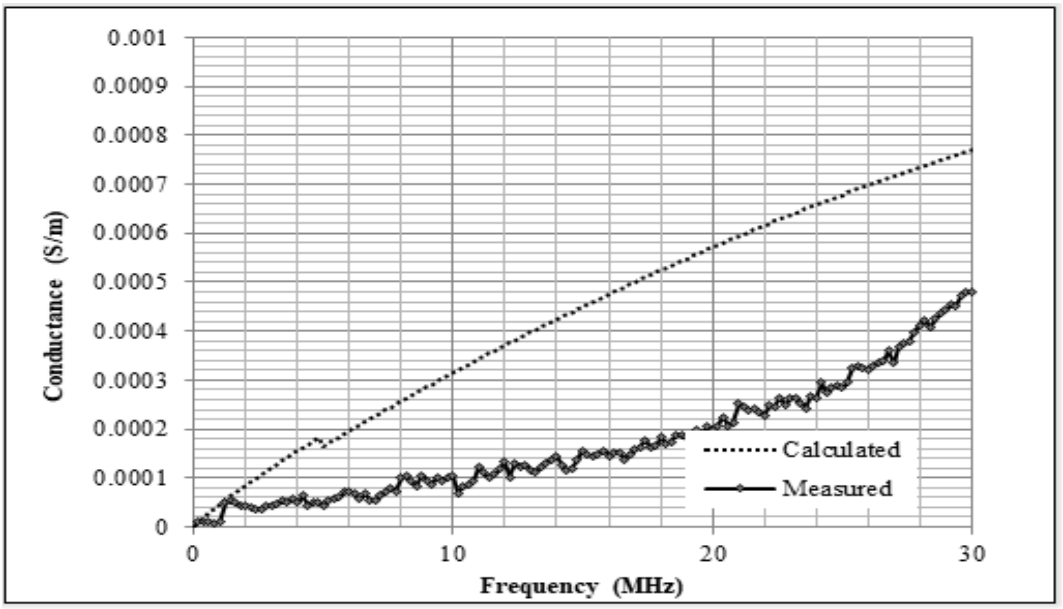

Figure 3.11: Conductance per unit length

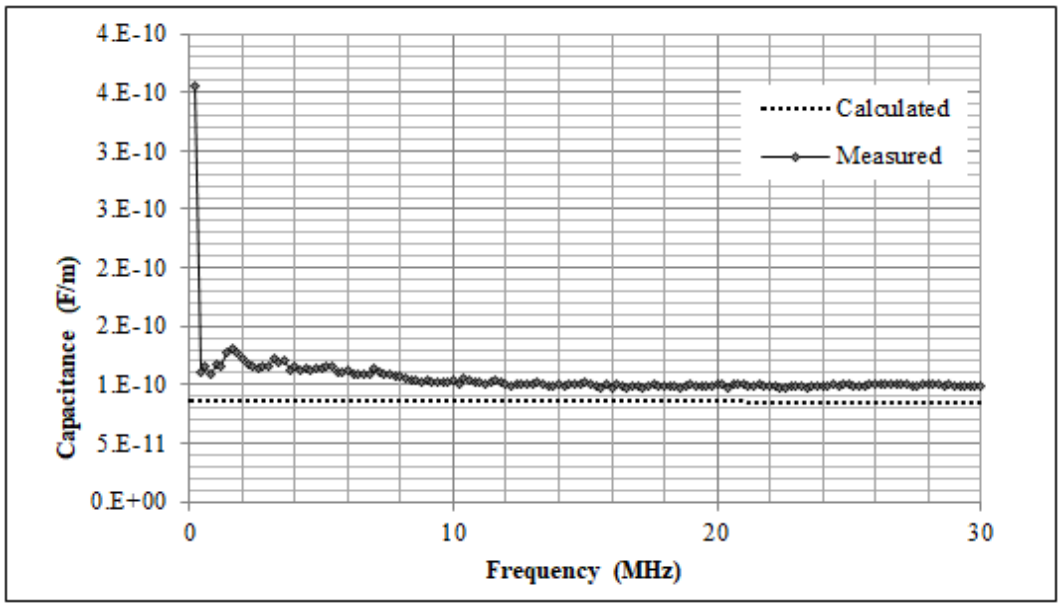

Figure 3.12: Capacitance per unit length

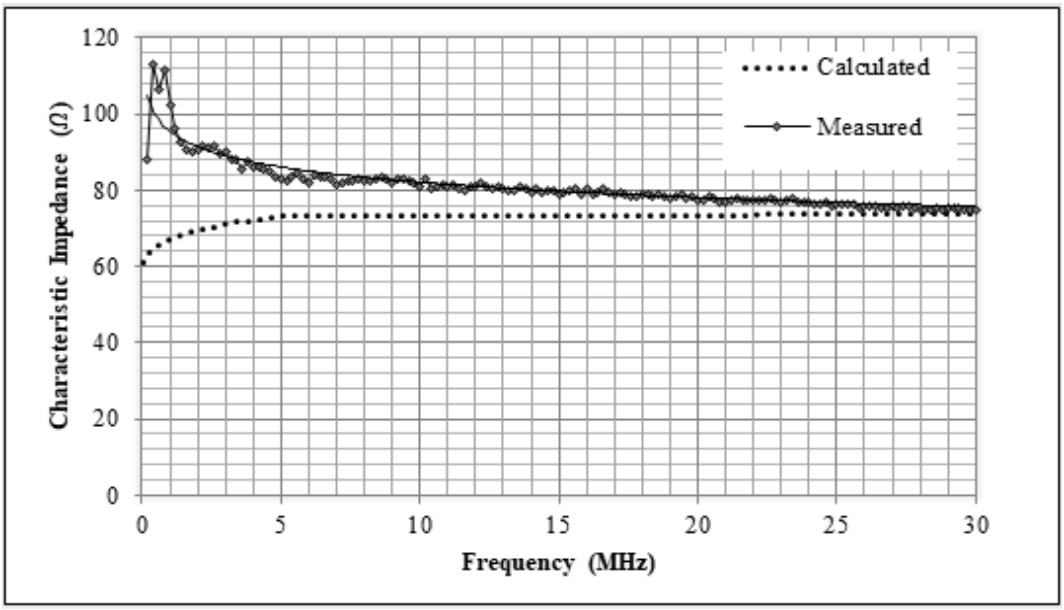

Figure 3.13: Characteristic Impedance

3.6 Propagation Velocity

The phase velocity υ_P, of a transmission line is important in determining the electrical wavelength of the signal λ, at different frequencies. Thus, a cable is considered to be short if its electrical length is less than $\frac{\lambda}{16}$ [77] or less than $\frac{\lambda}{8}$ [78] in which case the voltage and current distribution is considered constant and hence transmission line analysis would not be necessary. The phase velocity can be determined as [56, 57]:

$$\upsilon_p = \lambda f \tag{3.22}$$

Also, υ_p in (3.22) can be determined from the dielectric constant ϵ_r and the relative magnetic permeability of the dielectric material μ_r as [79]:

$$\upsilon_p = \frac{c_o}{\sqrt{\epsilon_r \mu_r}} \tag{3.23}$$

where c_o is the speed of light in free space. In [76], the approximate value for phase velocity in PVC cables is 0.5 c_o. The measured and calculated values of the phase velocity is as shown in Figure 3.14.

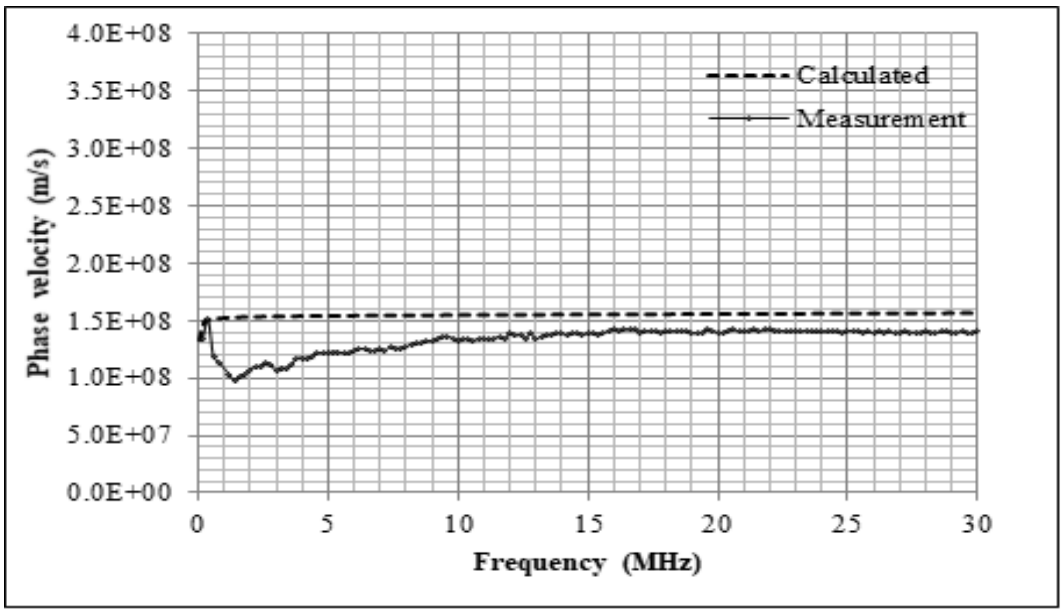

Figure 3.14: Phase velocity

3.6.1 Attenuation Constant

The real part of the propagation constant derived in (2.32), is the attenuation factor which is used to determine the power line attenuation factor of the direct path between the transmitter and the receiver. The measured results for the attenuation constant are shown in Figure 3.15.

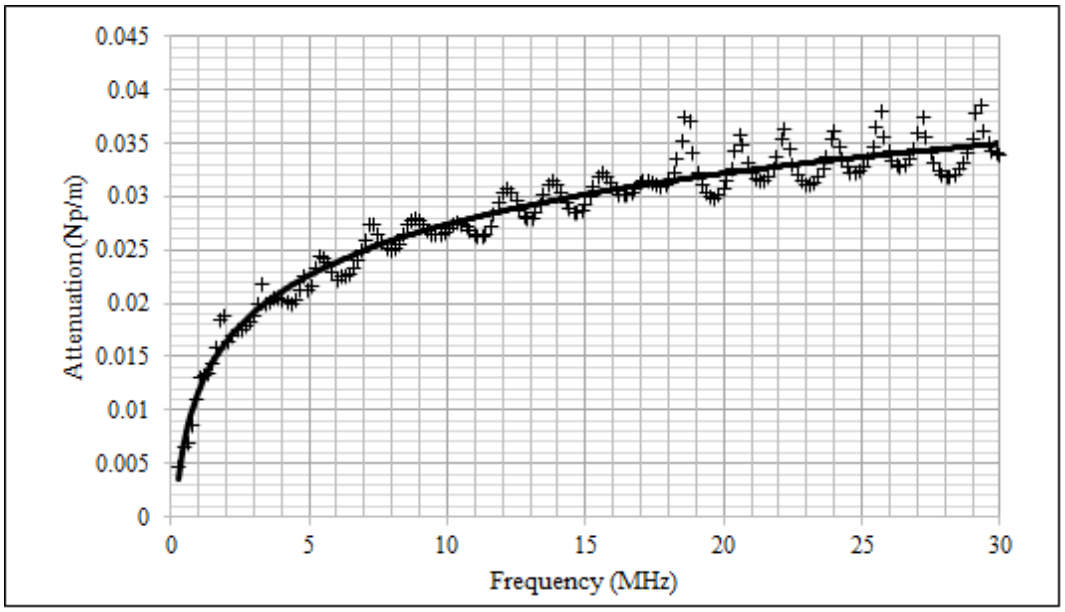

Figure 3.15: Attenuation constant

3.7 Chapter Summary

In this chapter, the extraction of primary line parameters that are used in the modeling of the input impedance of the PLC channel in chapter 4 have been discussed. The theoretical and measurement methods of line parameter extraction have also been described in detail. Oscillations are seen to occur at lower frequencies in the open and short-circuit terminated input impedance measurements that are seen to disappear at higher frequencies, meaning that the line used to determine the line parameters must be electrically short. Due to variation in the the properties of the PVC cables, deviations are seen between the measured and theoretical values of the resistance and conductance parameters.

Chapter 4

MODELLING AND CHARACTERISATION OF PLC CHANNEL IMPEDANCE

4.1 Introduction

The already established and extensive infrastructure of the power line network and the ever increasing demand for telecommunication services makes power line communication (PLC) a very attractive mode of data transmission [47, 55]. Power line cables are designed for the transmission of high voltage at low frequencies contrary to the low voltage at high frequencies needed for data transmission. Electric devices are also randomly connected and disconnected in and out of the power line network. This in turn results in varying network impedance, considerable noise and high attenuation [50], [55], [80], [81]. The heterogeneous nature of wiring practices, loads connected to the PLC network with unmatched impedance to the feed lines and branches connected to the network also result in impedance mismatch. Currently, there are different studies on the varying impedance of a PLC network [82]. Bushra Rasool et al. [83] presented a statistical model of the behaviour of the PLC impedance for a frequency range of 3–148.5 kHz in the narrowband and 1–35 MHz in the broadband PLC networks with varying load types. Tanaka [84] performed measurements and determined impedance characteristics, transmission loss and noise power spectrum of the power line for a frequency range of 10 kHz–100 MHz. In the narrowband PLC, Nicholson and Malack [85] carried out power line impedance measurements of unfiltered commercial power sources for a frequency band of 20 kHz–30 MHz. Vines et al. [86] also carried out measurements of the power line impedance for a frequency range of 5–20 kHz. Impedance measurement campaign was carried out for power lines in rural, urban and industrial areas in Turkey for a frequency band of 10–170 kHz in [87]. Although the various studies on the power line impedance have been performed, more data is needed and as it will serve as a good tool for optimum modem design. This chapter presents modeling of input impedance in a power line channel using parallel resonant circuits. It also aims to establish the effect of the branch lengths, number of branches and the terminating load impedances on the input impedance of the power line network. A description of the extraction of the power line cable parameters used for the test networks is provided. The input impedance of the power line network is then modeled and the model parameters are determined. The analysis and profiling of the input impedance using the model described

is then carried out and the model results are compared to measurements.

4.2 Power Line Network Impedance Model

The indoor power line network is composed of numerous branches. From the mains supply, the power line then branches into various sections which then terminates at different socket outlets. The branches are of different lengths and are terminated by different loads. The parallel resonance model considers the load branches as generalised parallel R-L-C circuits. Considering a parallel R-L-C circuit connected to a transmission line with characteristic impedance Z_o shown in 4.1, the frequency dependent input impedance seen by the input signal can be determined as [56]:

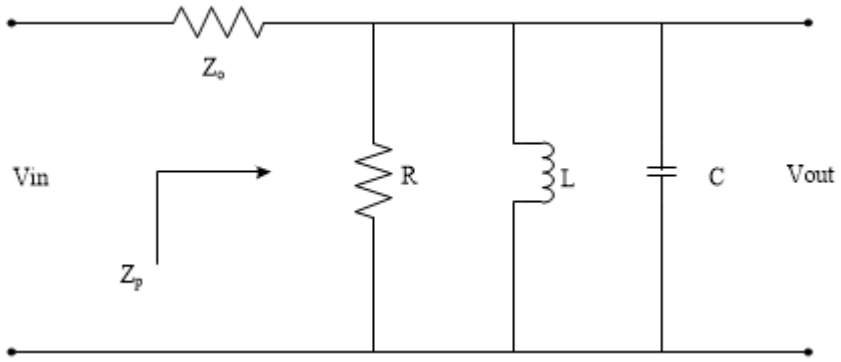

Figure 4.1: Parallel resonant circuit branch

$$Z_p = \left(\frac{1}{R} + \frac{1}{\jmath\omega L} + \jmath\omega C \right)^{-1} \tag{4.1}$$

while the complex power delivered to the resonator will be:

$$P_{in} = \frac{1}{2}|V|^2 \left(\frac{1}{Z_p} \right) \tag{4.2}$$

where V denotes the input voltage. Also, the power dissipated by the resistor R, will be defined as:

$$P_{loss} = \frac{1}{2R}|V|^2 \tag{4.3}$$

If the average magnetic energy stored in the inductor is W_m and the average electric energy stored in capacitor is W_e , the quality factor can be expressed as [56]:

$$Q_o = \omega_o \frac{W_m + W_e}{P_{loss}} \tag{4.4}$$

Therefore, at resonance $W_m = W_e$ where ω_o is the angular resonant frequency and thus, the quality factor for a parallel resonant circuit will be determined as:

$$Q_o = \frac{R}{\omega_o L} = \omega_o RC \tag{4.5}$$

The input impedance in (4.1) will then be written as:

$$Z_p = \left(\frac{1}{R} + \jmath\omega C\left(\frac{\omega^2 - \omega_o^2}{\omega^2}\right)\right)^{-1} \tag{4.6}$$

for $\frac{\Delta\omega}{\omega_o} \ll 1$, $\omega^2 - \omega_o^2 \approx 2\omega\Delta\omega$. Thus, Z_p can be expressed as [56]:

$$Z_p = \frac{R}{1 + \jmath\frac{2\Delta\omega Q_o}{\omega_o}} \tag{4.7}$$

4.2.1 Determination of Model Parameters

The parallel resonant circuit can be obtained by employing the transmission line theory for short and open- circuit terminated lines. The length of the cable is in even multiples of $\frac{\lambda_o}{2}$ for an open-circuit terminated line and odd multiples of $\frac{\lambda_o}{4}$ for short-circuit terminated line [57] where λ_o is the wavelength at resonance. Thus the input impedance of the open-circuit terminated transmission line of length, l, with a characteristic impedance, Z_o, attenuation constant, α, and phase constant, β, will be [56, 57]:

$$Z_{in} = Z_o\frac{1 + \jmath tan\beta l \tanh\alpha l}{\tanh\alpha l + \jmath tan\beta l} \tag{4.8}$$

for $\alpha l \ll 1$; $\tanh\alpha l = \alpha l$:

$$Z_{in} = Z_o\frac{1 + \jmath\alpha l tan\beta l}{\alpha l + \jmath tan\beta l} \tag{4.9}$$

The input impedance in (4.9) can be simplified near resonance by letting $\omega = \omega_o + \Delta\omega$, where $\Delta\omega$ is small and v_p is the phase velocity. Thus:

$$\beta l = \frac{\omega_o l}{v_p} + \frac{\Delta\omega l}{v_p} \tag{4.10}$$

At a half wavelength:

$$\beta l = \pi + \frac{\Delta\omega\pi}{\omega_o} \tag{4.11}$$

$$\tan\beta l = \tan\left(\pi + \frac{\Delta\omega\pi}{\omega_o}\right) \approx \frac{\Delta\omega\pi}{\omega_o} \tag{4.12}$$

Substituting (4.12) into (4.9) and assuming $\jmath\alpha l\Delta\omega\pi/\omega_o \ll 1$ gives [56, 57]:

$$Z_{in} = Z_o\left(\frac{1+\jmath\alpha l\frac{\Delta\omega\pi}{\omega_o}}{\alpha l+\jmath\frac{\Delta\omega\pi}{\omega_o}}\right) \tag{4.13}$$

$$Z_{in} = \frac{Z_o}{\alpha l+\jmath\frac{\Delta\omega\pi}{\omega_o}} \tag{4.14}$$

This result is the same as for the parallel resonant circuit derived in (4.7). Thus, a half-wavelength long open-circuited transmission line is similar to a parallel resonant circuit. The resistance, inductance and capacitance of the equivalent R-L-C circuit can therefore be identified as [56, 57]:

$$R = \frac{Z_o}{\alpha l} \tag{4.15}$$

$$L = \frac{2Zo}{\pi\omega_o} \tag{4.16}$$

$$C = \frac{\pi}{2\omega_o Z_o} \tag{4.17}$$

For the short-circuit terminated line, the input impedance can be determined as [56, 57]:

$$Z_{in} = Z_o\left(\frac{1-\jmath\tanh\alpha l\cot\beta l}{\tanh\alpha l-\jmath\cot\beta l}\right) \tag{4.18}$$

The equivalent input impedance for the short-circuit terminated line near resonance, can be obtained through the same procedure as [56, 57]:

$$Z_{in} = \frac{Z_o}{\alpha l+\jmath\frac{\Delta\omega\pi}{2\omega_o}} \tag{4.19}$$

The resultant input impedance in (4.19) is observed to be similar to that derived in (4.7) and thus, a quarter-wavelength long short-circuited transmission line is similar to a parallel resonant circuit. The equivalent resistance, inductance and capacitance of the equivalent

R-L-C circuit can then be identified as [56, 57]:

$$R = \frac{Z_o}{\alpha l} \tag{4.20}$$

$$L = \frac{4Zo}{\pi \omega_o} \tag{4.21}$$

$$C = \frac{\pi}{4\omega_o Z_o} \tag{4.22}$$

4.2.2 Input Impedance

Previous contributions have proposed modelling power line channels as a cascade of decoupled resonant circuits [47, 50, 51]. In [51], the power line channel has been modeled as a cascade of parallel resonant circuits where the overall transfer function of the network is determined as:

$$H(f) = A \prod_{i=1}^{N} H_{pi}(f) \tag{4.23}$$

where H_{pi} is the transfer function of the i_{th} resonant circuit and N denotes the number of parallel resonant circuits in the network. A is the power line attenuation factor of the direct path between the transmitter and the receiver, and depends on the frequency and length of the line given by [43, 50]:

$$A_{(f,l)} = e^{-\alpha_{(f)} l} \tag{4.24}$$

where α denotes the attenuation constant of the power line and l is the length of the direct path between the transmitter and the receiver. For each resonant circuit, the transfer function is determined as [51]:

$$H_p(f) = \frac{V_{out}}{V_{in}} = \frac{Z_o}{Z_o + Z_p} \tag{4.25}$$

where Z_o is the line characteristic impedance and Z_p is the frequency dependent input impedance of each resonant circuit. Thus the transfer function depends on the impedance of the power line channel and can be re-written as [52, 88]:

$$H(f) = A\left(\frac{Z_o}{Z_o + Z_{(f)}}\right) \tag{4.26}$$

Therefore, from (4.14) the overall resultant frequency dependent input impedance of a given network can be determined as [88]:

$$Z_{(f)} = \left(\frac{AZ_o + H(f)Z_o}{H(f)}\right) \tag{4.27}$$

The electrical length of the branch can be expressed in terms of the wavelength λ and is related to the phase velocity υ_p and the operating frequency f by [88, 89]:

$$\lambda = \frac{\upsilon_p}{f} \tag{4.28}$$

The first resonant point for a branch terminated by an open-circuit will occur at a resonant frequency relative to the branch length, l, given as [50, 88]:

$$f_o = \frac{\upsilon_p}{4l} \tag{4.29}$$

The subsequent peaks along the open-circuit branch will occur at [51, 88]:

$$f_{on} = \frac{\upsilon_p}{4l}(2n+1), n = 1, 2, 3\ldots \tag{4.30}$$

For a branch terminated by short-circuit, the first resonant point will occur at zero with the subsequent points given by [51, 88]:

$$f_{sn} = \frac{\upsilon_p}{4l}(2n), n = 1, 2, 3\ldots \tag{4.31}$$

where υ_p denotes the phase velocity.

4.3 Methodology and Experimental Set-up

The TR5048 vector network analyser was used to obtain impedance measurements for a frequency band of $1 - 30$ MHz that was used to evaluate the validity of the model. The power line networks were connected to the network analyser via differential mode passive circuitry at both the transmitting and receiving ends to couple the communication signals onto and from the powerlines. One path two port calibration was done by the use of 53K36R-MSON3 calibration kit so as to ensure high accuracy and integrity of measurements as the analyser measurement capability is for S_{11} and S_{21} parameters. The

reference port impedance for the network analyser is 50 Ω. The test networks are as illustrated in Figures 4.2 through 4.4. The branches are open-circuit terminated with the transmitter and receiver located at point A and B, respectively in all cases.

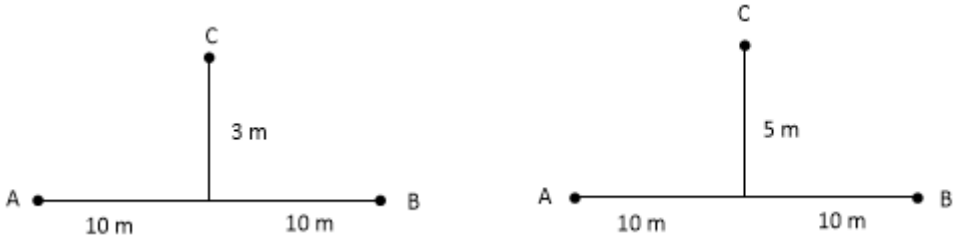

(a) Network A (b) Network B

Figure 4.2: Single branch networks

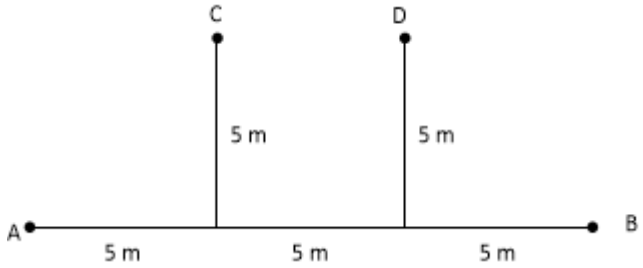

Figure 4.3: Network C

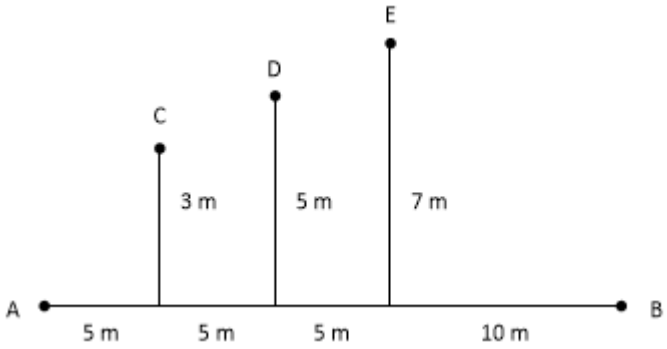

Figure 4.4: Network D

The input impedance for the different networks were then obtained from the network analyser through port impedance conversion function that converts the the S-parameters measured at 50 Ω port into values which would be found if measured at at a test port with arbitrary impedance.

4.4 Results and Discussion

The results for the measured and model impedance are as depicted in Figures 4.5,4.6, 4.9 and 4.10 respectively. The results for the single branched network for the 7 m and 10 m

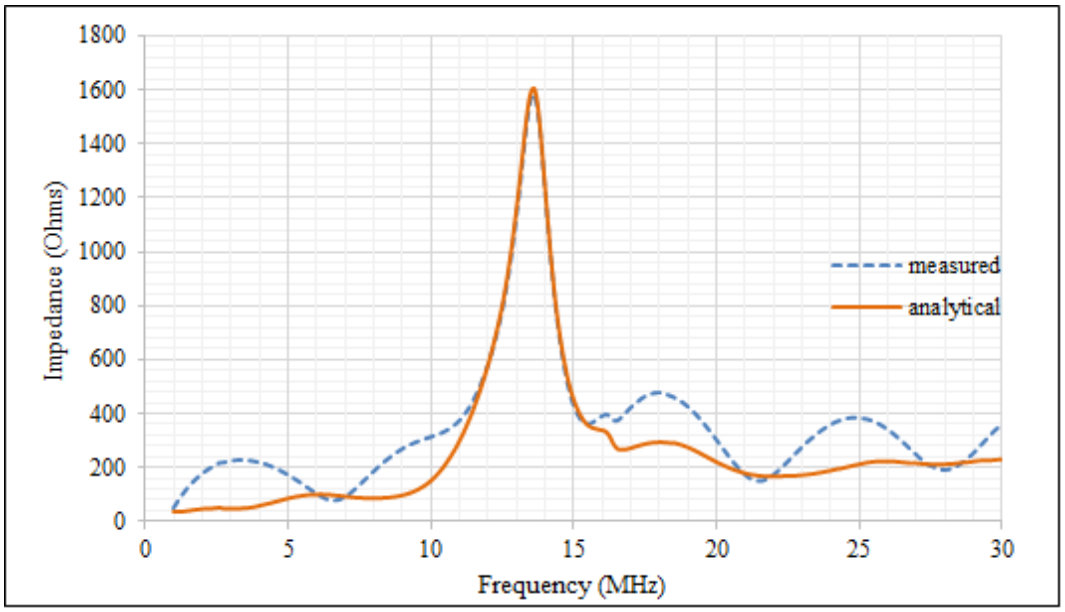

Figure 4.5: 3m branch

branches with the same configuration were also obtained and are shown in Figure 4.7 and Figure 4.8 respectively.

The network impedance varies with frequency with the peaks occurring at resonant frequencies 4.30. These peaks correspond to the resonant points as described by the parallel resonant circuits with open-circuit termination where the impedance is maximum. When the length of the branch is increased from 3 m–10 m, the number of peaks in network impedance also increases as shown in Figures 4.5 through 4.8. The length of the branch also determines the position of the peaks in the network impedance profile. For longer branches, the resonant points start at lower frequencies than those of shorter branches

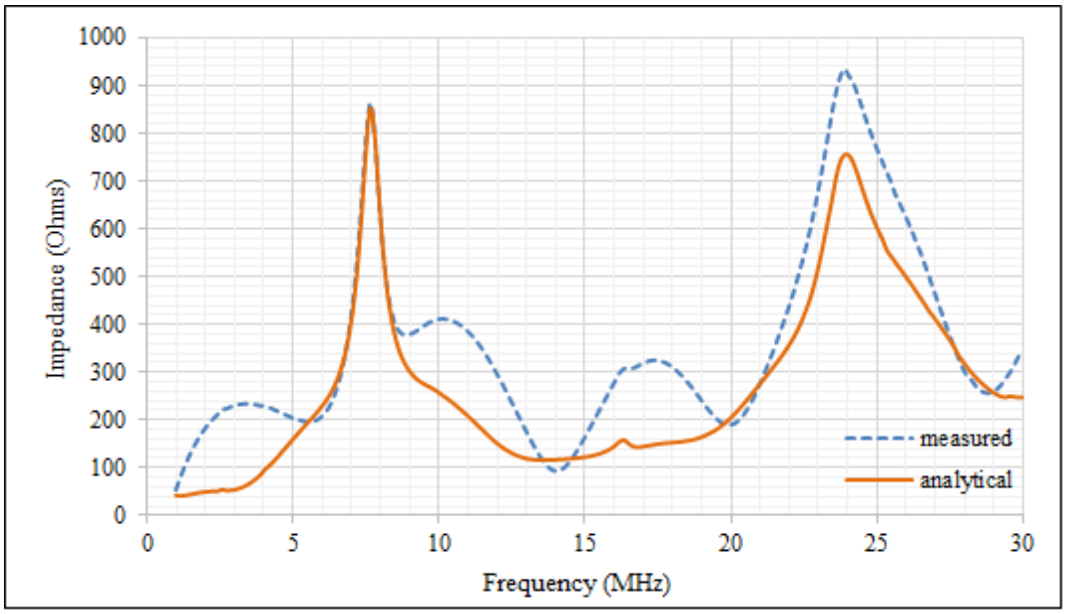

Figure 4.6: 5m branch

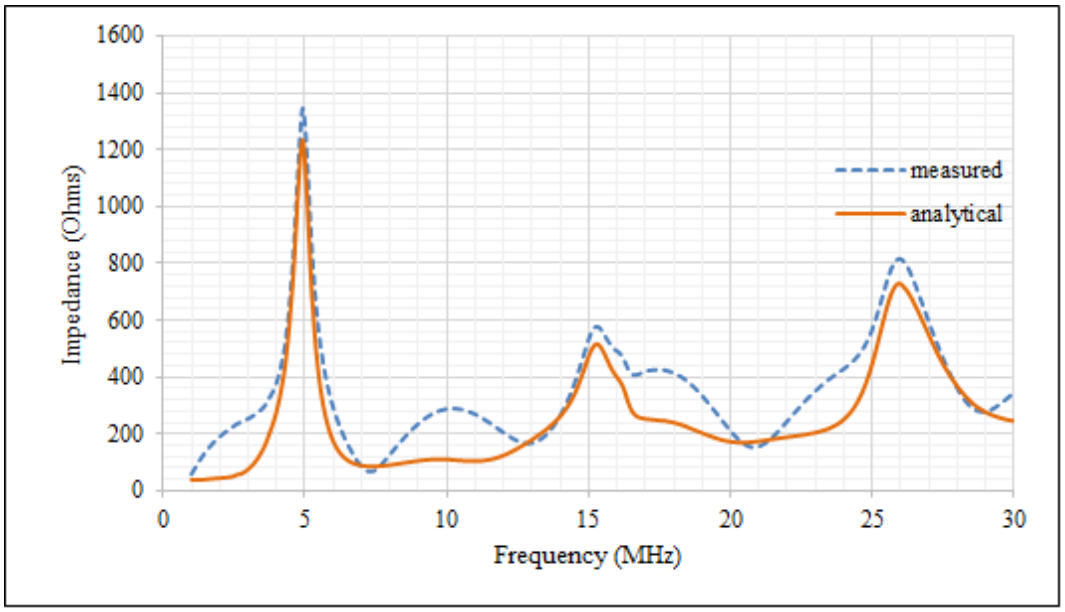

Figure 4.7: 7m branch

4.29. The first peak for the 5 m branch is observed at a frequency of 8 MHz while that of the 7 m branch is at 5 MHz frequency. As shown in Figures 4.6 and 4.7 respectively. The effect of the branch length on the network impedance is summarize in Table 4.1.
It is observed that the number of branches determines the magnitude of the input impedance of the network. As the number of branches increase the magnitude of the network impedance also increases. For the 3 m branch in Figure 4.5, the magnitude maximum peak is 1.6 kΩ while for network D, the magnitude of the maximum peak is 6.1 kΩ as shown in Figure 4.10.

When the length of the branches are equal, the peaks occur at the same resonant frequencies as they do for a single branch with the same length but with a higher value of the input impedance. This is observed in Figures 4.6 and 4.9 where the peaks occur at 7.6 MHz and 24 MHz for network B and network C topologies. When the branches have different lengths, the peaks are seen at points corresponding to the resonant frequencies of the individual branch lengths 4.9.

Table 4.1: Effect of Branch length on the Network Impedance

Branch Length	Number of Peaks	Position of First Peak
3 m	1	13.6 MHz
5 m	2	7.6 MHz
7 m	5	4.9 MHz
10 m	4	3.9 MHz

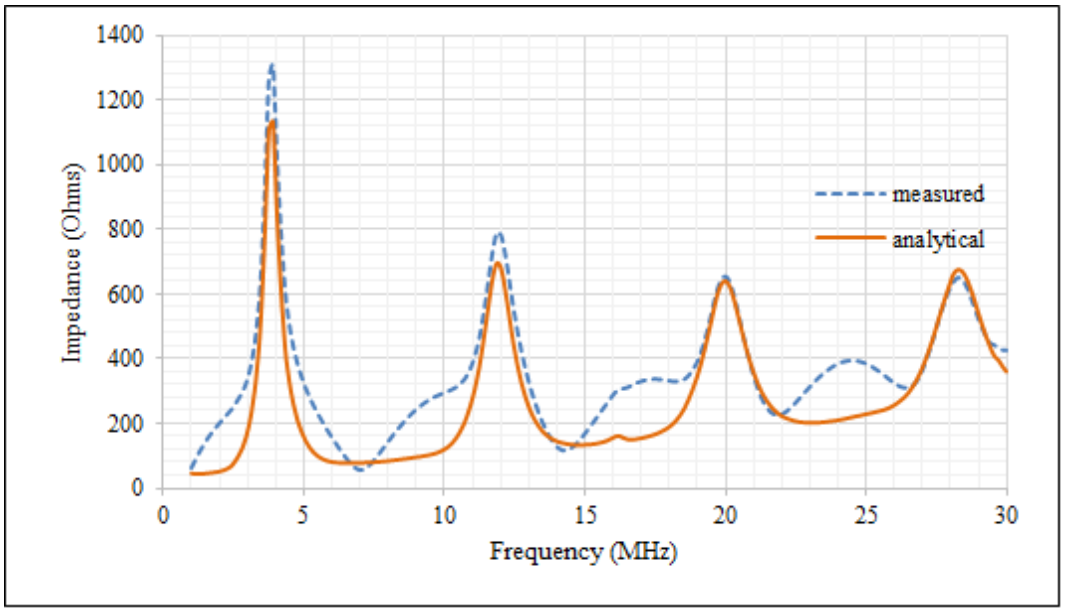

Figure 4.8: 10m branch

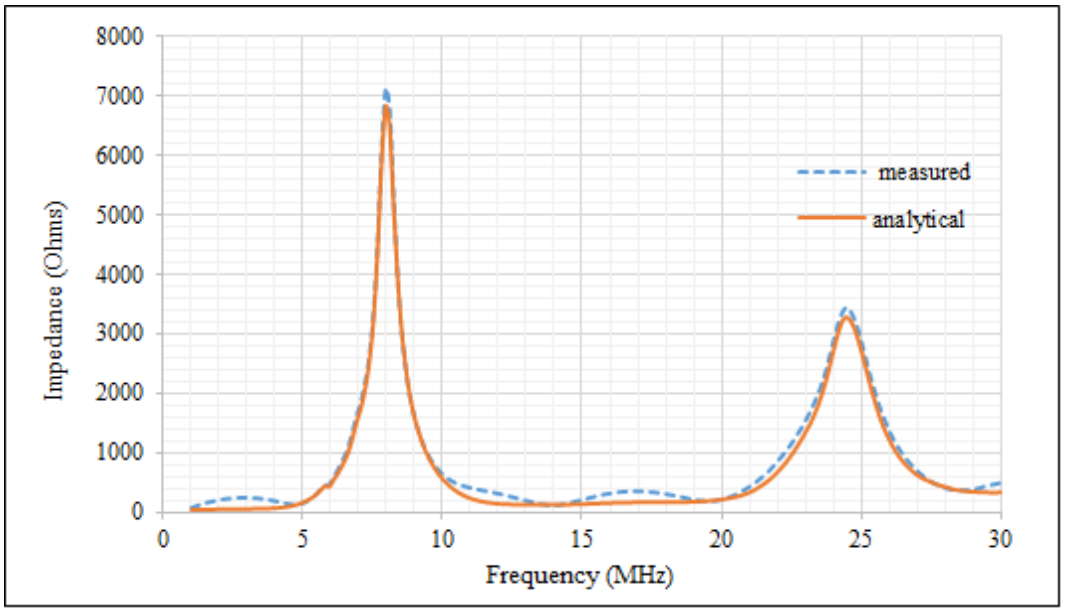

Figure 4.9: Two-branches

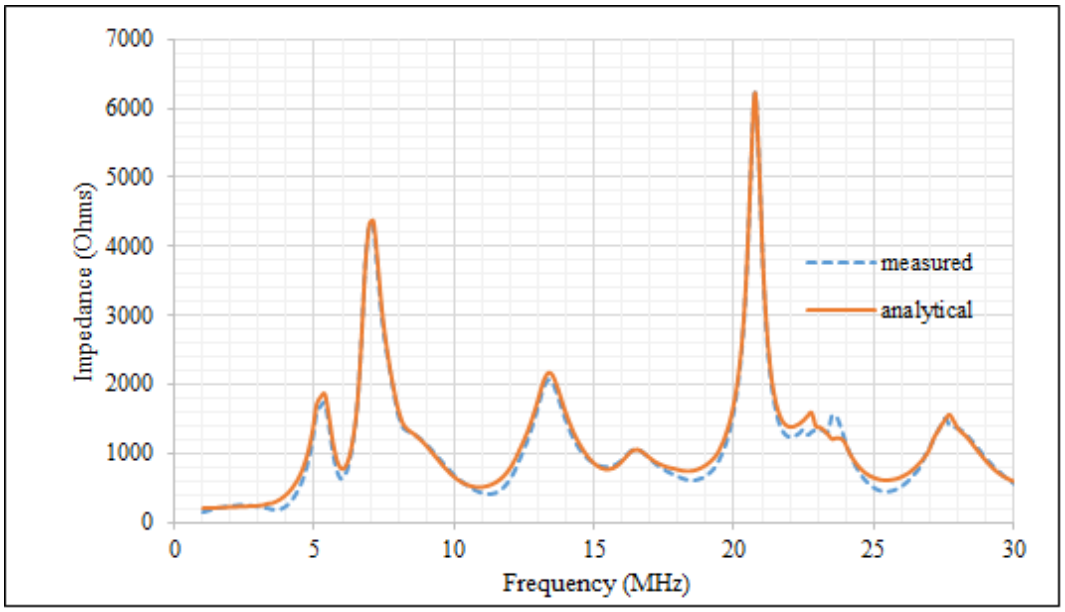

Figure 4.10: 3-branched network

4.5 Impedance Profiling

The minimum, average and maximum input impedance values for the entire network for single branch networks with different branch lengths are summarized in Table 4.2. The minimum bounds for the network input impedance range from 52 Ω to 58 Ω which is close to 50 Ω reference port impedance of the network analyzer. As observed from Table 4.2, the average impedance remains the same through different branch lengths at about 354 ± 1.1 % Ω. The average impedance for a two-branch network and three-branch network show in Figure 4.9 and Figure 4.10 respectively was determined for the entire network in each case. The average impedance obtained were 862.69 Ω and 1124 Ω for the two cases respectively. The average impedance values differ significantly from those in Table 4.2. Therefore, we can conclude that the result presented in Table 4.2 is peculiar with indoor single branch networks. This can be considered in the design of impedance matching networks. The maximum values of the input impedance fluctuate with 933 Ω as the value of the smallest peak and 1586 Ω as as the highest peak for the 3 m branch depicting the unpredictable nature of the input impedance.

Table 4.2: Input Impedance Bounds

Branch Length	Minimum	Average	Maximum
3 m	52 Ω	351 Ω	1586 Ω
5 m	55 Ω	357 Ω	933 Ω
7 m	58 Ω	350 Ω	1342 Ω
10 m	56 Ω	353 Ω	1310 Ω

4.6 Summary

In this chapter, we have modelled and profiled the input impedance of a PLC network using parallel resonant circuits. The worst case scenario of open was considered. For the short-circuit, the behaviour would be the exact opposite to that of the open-circuit. The inpit impedance has been modelled using the transmission line theory. From the analysis and measurements performed, the uloaded transmission lines are confirmed to behave similar to the parallel resonant circuit. The length of the branch determines the frequencies at which the input impedance is maximum that is, at resonant frequencies, which also depend on the phase velocity. As the branch length increases, the number of resonant points increases as well and hence the number of peaks. The highest peaks are observed at resonant frequencies. Although longer branches have more peaks as compared to shorter branches, the average values of the input impedance for single branched networks fall at approximately the same range in the frequency band of $1 - 30$ MHz.

Chapter 5

DESIGN OF A BIDIRECTIONAL IMPEDANCE ADAPTIVE COUPLER

5.1 Introduction

Power line communication as a mode of transmission of high-frequency signals, presents a cost effective solution due to the ubiquitous infrastructure and is set to change the largest existing network, the power line grid, in to a data transmission network. On the other hand, it presents a harsh environment to the propagating high frequency signal due to the time varying nature of the line impedance and impedance mismatch caused by varying loads connected to the network as it is not designed for high speed transfer of data [68,90]. The high-frequency communication signal needs to be superimposed onto and/or extracted from the power line network. This is achieved by using a coupler. The coupler also functions as a filter for the mains voltage as well as matching circuit to the input impedance of the power line network. The latter function is not always encoporated, as most coupling circuits are basically highpass and/or bandpass filters, as shown in [90–93]. For optimum modem design, the power line input impedance must be known in order to maximize power transfer between the input and output ports of the communication device and the power line through impedance matching [87]. A lot of research on power line coupling has been in narrowband [90], and the transformerless bandpass couplers developed in [91] provide a smaller band for matching. Therefore there is need to to design and build a power line coupler that filters the low frequency mains supply as well as accomplish matching over a wider band for broadband PLC applications.

The objective of this chapter is to design a bidirectional adaptive impedance matching coupler for broadband PLC applications. The matching section of the coupler is designed such that it has the characteristics of a lowpass filter while the coupling section is a highpass filter, collectively forming a bandpass network. Both the matching and the coupling sections are designed using passive filters. This chapter is organised such that it begins with the design of the matching circuit using L-section configurations. The design of the highpass filter is built by cascading two T-networks to form a Pi-network which is later bisected such that each half is connected to either port of the communication device to filter out the mains supply. The parameters of the highpass filter are then obtained through the transmission line parameters of the two-port network. The designed circuit

is first simulated to evaluate its transfer characteristics which are then validated with measurements for the frequency range of 1–30 MHz.

5.2 Matching Circuit Design

The power line network is basically designed for the transfer of high voltage at a low frequency, whereas the transfer of communication signals requires low voltage and high frequency. The loads connected to and disconnected from the network also pose a major challenge of impedance variation in the power line network [62]. Measurement results show that the input impedance of the power line network varies from a few Ohms to a few kilo Ohms. In this work, the power line impedance is characterised and profiled as minimum, average and maximum in the frequency range 1-30 MHz, as shown in Table 4.2. The power line input impedance is also observed to have an unpredictable nature as the peak values of the input impedance do not necessarily depend on the length of the branch connected to the power line network. This variation in the PLC network impedance results in impedance mismatch, leading to poor power transfer from the source to the load and high signal reflection. From Table. 4.2, the average value of the PLC network impedance is found to be 354 $\pm$ 1.1 % Ω whereas the maximum values fluctuate between 933 Ω and 1586 Ω. It is therefore necessary to match the 50 Ω transmitter and receiver impedance with the power line impedance in order to ensure maximum power transfer.
From the maximum power transfer theorem in time varying wave-forms, maximum power from the source to the load occurs when the source impedance is equal to the complex conjugate of the load impedance. This can be achieved by impedance matching where the load is forced to "look-like" the complex conjugate of the source using reactive components where power dissipation is ideally zero but matching is frequency dependent. In this case, the source is conjugate matched at the input of the network and the load is conjugate matched at the output of the network; that is, if the source $Z_s = R_s + \jmath X_s$, the load will be $Z_l = R_l - \jmath X_l$. Therefore, the net reactance of the loop (matching section) will be zero and $R_s = R_l$. From Figure 5.1, the reactance between R_s and R_l reduces the current in R_l, thus reducing the power dissipated at the load.

Impedance matching using reactive components can be done using a simple L-section configuration that utilises two reactive components. One of of the reactive components is

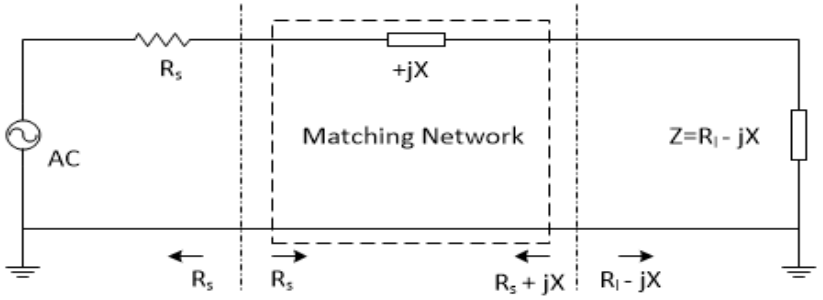

Figure 5.1: Impedance matching for maximum power transfer

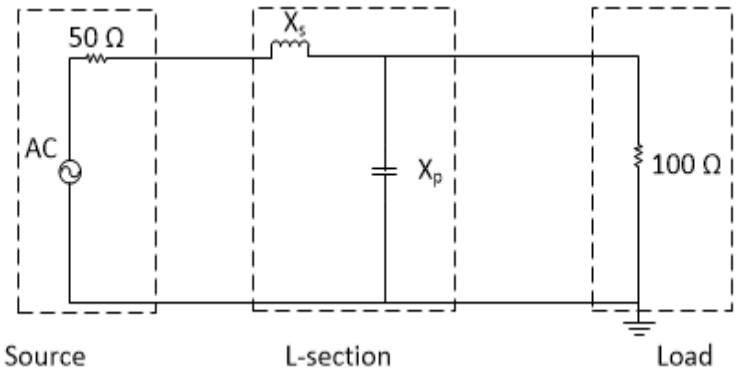

Figure 5.2: L-section matching circuit

connected in parallel with larger load in order to transform it into a smaller value as the resultant value of the two will be smaller. The other reactive component is connected in series with the smaller load and thus the resultant impedance at that section will be the addition of the two impedances in series transforming it to a larger value. The L-section matching circuit with a source and a load is as shown in Figure 5.2.

Assuming that a source impedance $Z_s = R_s + jX_s$ is the complex conjugate of the load impedance $Z_l = R_l + jX_p$, it can be shown that:

$$\sqrt{R_s^2 + X_s^2} = \frac{X_p R_l}{\sqrt{R_l^2 + X_p^2}} \tag{5.1}$$

The quality factor Q, of the reactive L-section circuit is defined as [57]

$$Q = \omega\left(\frac{Energy\ stored\ in\ the\ network}{average\ power\ loss}\right) \tag{5.2}$$

where ω is the angular frequency of the signal. Thus, for the series circuit $Q = \frac{X_s}{R_s}$ and for the parallel circuit, $Q = \frac{R_l}{X_p}$. Assuming that the quality factor for the series and the parallel circuits are equal and substituting X_s and X_p into (5.1) we get [57]:

$$\sqrt{R_s^2 + (QR_s)^2} = \frac{\frac{R_l^2}{Q}}{\sqrt{R_l^2 + (\frac{R_l}{Q})^2}} \tag{5.3}$$

Equation (5.3) can further be simplified to:

$$Q^2 + 1 = \frac{R_l}{R_s} \tag{5.4}$$

Therefore, for a resistive load to be matched to another resistor, R_l and R_s are defined such that $R_l > R_s$ and the quality factor can then be calculated from (5.4). Thus, for the L-section matching circuit in Figure 5.2, $R_s = 50\ \Omega$ and $R_l = 100\ \Omega$. The Q-factor and

the reactive components can then be found as: $Q = \sqrt{\frac{R_l}{R_s} - 1} = 1$, $X_s = QR_s = \jmath 50\ \Omega$ and $X_p = \frac{R_l}{Q} = -\jmath 100\ \Omega$. The load impedance is determined as $Z_l = X_p \parallel R_l = 50 - \jmath 50\ \Omega$. The resultant matching circuit is shown in Figure 5.3. Thus, a parallel combination of a 100 Ω load and a 100 Ω capacitor will "look like" a series combination of a 50 Ω load and a 50 Ω capacitor.

Impedance matching in a power line network is effected at the coupler such that the 50 Ω

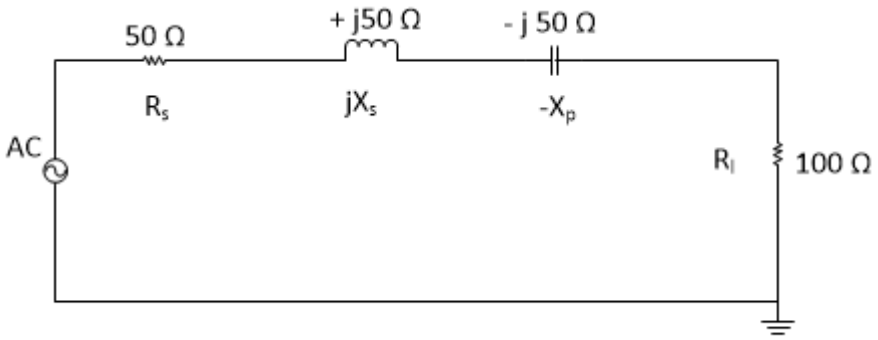

Figure 5.3: L-section matched circuit

transmitter and receiver ports see an impedance value that matches their own. For the simple RLC resonant discussed in chapter 2, the quality factor Q_{res} was determined as:

$$Q_{res} = \frac{f_o}{2\Delta f} = \frac{f_o}{2(Bandwidth)} \tag{5.5}$$

The L-section matching network in Figure 5.2, is equivalent to the RLC circuit but it also has a non-zero source connected in series which is matched to the load. Therefore Q will be twice Q_{res} and can be given as [94]:

$$Q = 2Q_{res} = \frac{f_o}{\Delta f} \tag{5.6}$$

Therefore, for a higher Q, the L-section network produces as narrowband match and a lower Q results on a widerband match. The variation of the bandwidth with the Q factor is as shown in Figure 5.4.

The use of one L section circuit has a limitation in that the quality factor of the circuit will solely depend on the source and the load impedance values, that is, once the source and the load impedance are defined, then the Q-factor is fixed resulting in a fixed bandwidth. Thus, the bandwidth provided by the L-section match may be either be too narrow or too wide depending on the application. For example, a narrow bandwidth is required when matching an antennae to a reciever so that signals from other stations do not overload the receiver while in other cases, a signal produced by a modulated transmitter may have greater bandwidth than the L-section would pass [94]. This problem can be solved by cascading two back-to-back L-section matching circuits to form either T-network or Pi-network.

Figure 5.5 shows the T-network matching circuit. Both the source and the load are

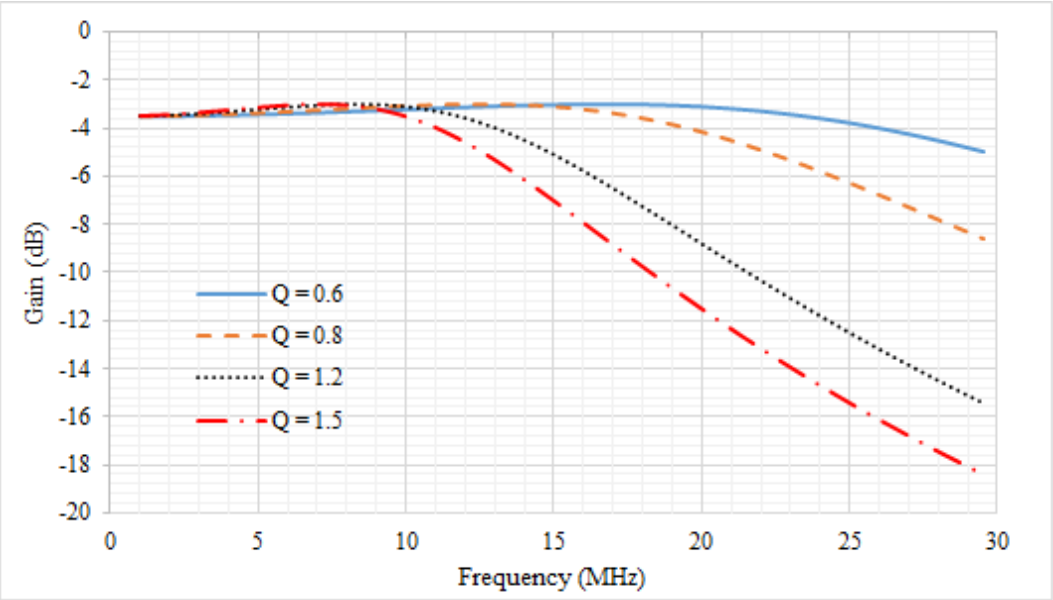

Figure 5.4: Response for different Q values

matched to a virtual resistor R_v where the series reactances are connected to the source and the load while the shunt reactances are connected in parallel to the virtual resistor. For the T-network, R_v must be greater than both the source and the load resistance. The source and the load resistances for the Pi-network shown in Figure 5.6 are also matched to R_v connected at the junction between the two cascaded L-section matching networks. In this case, the shunt reactances of the L-section networks are connected in parallel both at the source and at the load, while the series reactances are connected in series with the virtual resistor. The virtual resistor must therefore be smaller than both the source and the load as the reactances connected in series with R_v will transform the center impedance to a larger value that matches both the source and the load.

The resultant T and Pi- networks allow the designer to vary the Q value due to the free parameter R_v (used to determine the center impedance), that can be chosen to depending on the required bandwidth specifications. However, the quality factor value chosen must be greater than the Q value obtained from one L section circuit alone. This is because

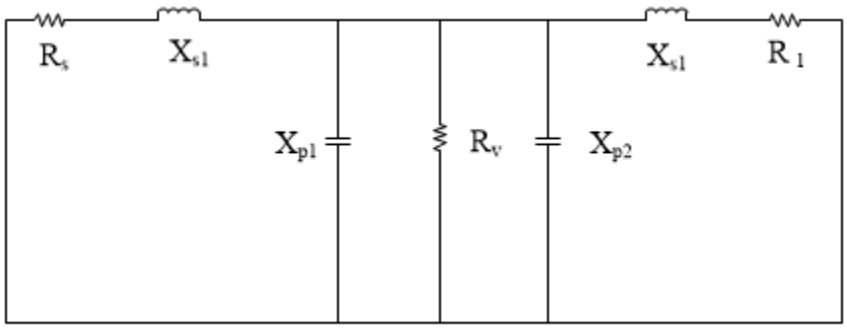

Figure 5.5: T-section Matching circuit

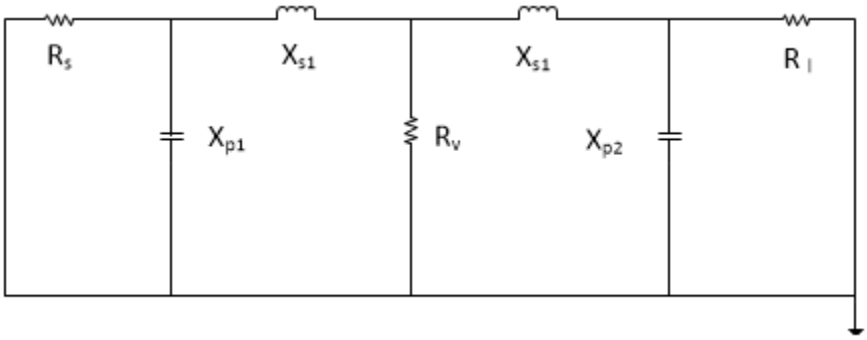

Figure 5.6: Pi-section Matching circuit

for the T-nework and Pi-network, R_v is greater or lower than both the source and the load resistance respectively. Assuming that the $R_s > R_l$ in both the Pi- network and T-network, then for the T-network:

$$Q_{Ts} = \sqrt{\frac{R_v}{R_s} - 1} \tag{5.7}$$

$$Q_{Tl} = \sqrt{\frac{R_v}{R_l} - 1} > \sqrt{\frac{R_l}{R_s} - 1} \tag{5.8}$$

Thus, the net Q will be greater than for a single L-section matching network, where Q_{Ts} and Q_{Tl} are the quality factors for the T-network for the source L-section and the load L-section matching circuit respectively. For the Pi-network:

$$Q_{Pis} = \sqrt{\frac{R_s}{R_v} - 1} > \sqrt{\frac{R_l}{R_s} - 1} \tag{5.9}$$

$$Q_{Pil} = \sqrt{\frac{R_l}{R_v} - 1} \tag{5.10}$$

Thus, the net Q for will be higher than for a single L-section matching circuit where where Q_{Pis} and Q_{Pil} are the quality factors for the Pi-network for the source L-section and the load L-section matching circuit respectively. This leads to a limitation of designing matching circuits with high quality factor, leading to narrower matched bands.
In order to achieve wider bandwidths in matching networks as well as versatility in the case of broadband power line communication, the value of Q must be low. The lowest value of Q is found by determining R_v as the geometric mean of the source and the load resistors [57], i.e. $Rv = \sqrt{(R_s R_l)}$ and thus $R_s < R_v < R_l$. In this type of matching, the load and the source are matched to a virtual resistor (R_v), connected at the junction of the two L-sections of the network as shown in Figure 5.7. The load R_l is assumed to be larger than the source R_s. Thus, the shunt reactance X_{p2} is connected to R_l in order to transform it to a smaller value while the series reactance X_{s1} is connected to $R_s$so as to transform it to a larger value. The series reactance X_{s1} and the shunt reactance X_{p1} and will cancel out as shown in Figure 5.3 following the same principle applied for the L-section matching circuit. The same case applies for the series reactance X_{s2} and the

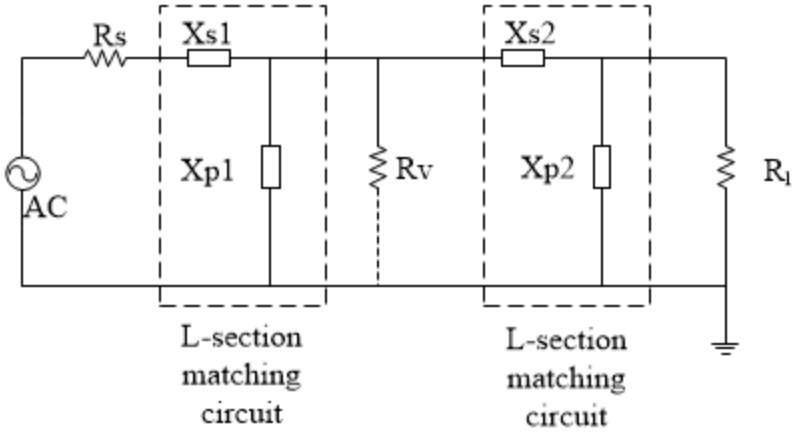

Figure 5.7: Matching circuit for low Q-factor

shunt reactance X_{p2}.

For broadband power line communication, the channel impedance is large compared to the transmitter or receiver impedance. Assuming a power line impedance R_l is 100 Ω is to be matched to a source impedance of 50 Ω, the impedance matching circuit is as shown in Figure 5.7. The virtual resistance $Rv = \sqrt{R_s R_l} = 70.71$ Ω. The quality factor for the load section $Q_l = \sqrt{\frac{R_l}{R_v} - 1}$ since $R_l > R_v$ and the quality factor for the source section is $Q_s = \sqrt{\frac{R_v}{R_s} - 1}$ since $R_v > R_s$; $Q_s = Q_l = 0.64$. The series reactances can thus be calculated as $X_{s1} = QR_s = 32$ Ω and $X_{s2} = QR_v = 45.25$ Ω. The shunt reactance $X_{p1} = \frac{R_v}{Q} = 110.5$ Ω and $X_{p2} = \frac{R_l}{Q} = 156.25$ Ω. Since the shunt and series reactances must cancel each other out, if X_{p1} is capacitive then X_{s1} must be inductive and vice versa. The same applies to X_{p2} and X_{s2}. The equivalent network is as shown in Figure 5.8. The component parameters are then determined from the upper cut-off frequency at which matching is to be achieved. The capacitance and the inductance values can be obtained as $C = \frac{1}{\omega_c X}$ and $L = \frac{X}{\omega_c}$ respectively, where ω_c is the upper angular frequency. The equivalent circuit is as shown in Figure 5.9.

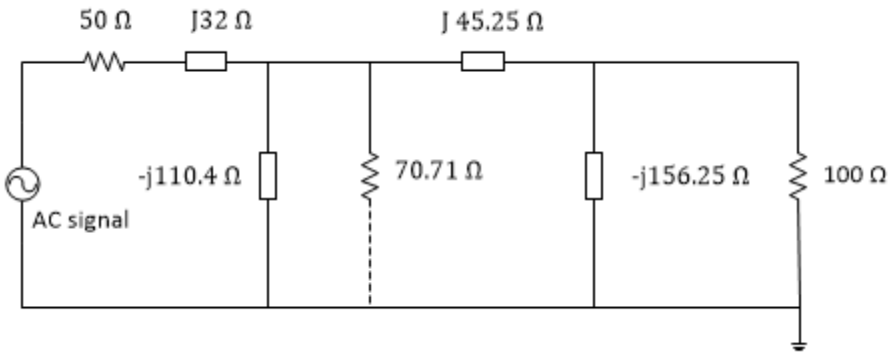

Figure 5.8: Equivalent matching network with a virtual resistor

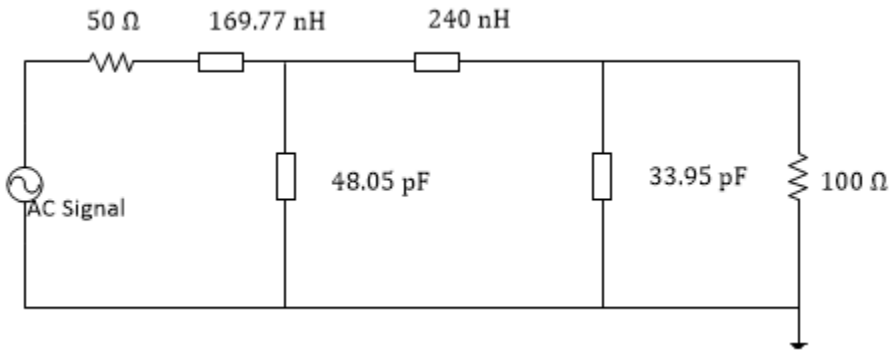

Figure 5.9: Equivalent circuit with component parameters

5.3 Coupling Circuitry

The PLC coupler filters the mains voltage preventing damage to communication devices and expensive measuring equipment. In general, couplers are either highpass or bandpass filters. In this design, the aim is to match the impedance of the source to the power line impedance for maximum power transfer as well as filter out the 50Hz mains signal to prevent it from damaging the communication devices. In order to achieve maximum power transfer, the source impedance (Z_s), the characteristic impedance of the coupler (Z_o) and the load (powerline) impedance (Z_l) must be equal i.e. $Z_s = Z_o = Z_l$. A symmetrical and reciprocal T-network is chosen for the design of the coupling circuit since it has properties of a bi-directional two-port network to allow selecting of any port as the input or output. The transmission parameters for the T-network A in Figure 5.10(a) are given by [57].

$$V_1 = AV_2 + BI_2 \tag{5.11}$$

$$I_1 = CV_2 + DI_2 \tag{5.12}$$

In the T- networks of Figure 5.10, port-1 is considered as the source and port-2 as the

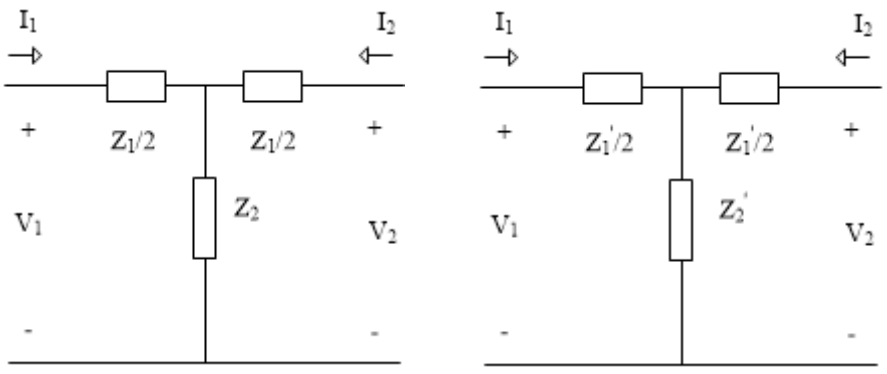

(a) T-section A (b) T-section B

Figure 5.10: T-networks

output. Therefore, the impedance at its input is given by:

$$Z_{in} = \frac{V_1}{I_1} = \frac{AZ_l + B}{CZ_l + D} \tag{5.13}$$

Since the network is symmetrical $A = D$ and $Z_{in} = Z_o = Z_l$, (5.13) can further be simplified to:

$$Z_{in} = Z_o = \sqrt{\frac{B}{C}} \tag{5.14}$$

The maximum power transfer function is therefore achieved through (5.14). The transmission parameters for the T-network are given by $B = Z_1 + \frac{Z_1^2}{4Z_2}$ and $C = \frac{1}{Z_2}$ [56,57]. Substituting B and C into (5.14) we get:

$$Z_o = \sqrt{Z_1 Z_2 \left(1 + \frac{Z_1}{4Z_2}\right)} \tag{5.15}$$

For a highpass T-section, $Z_1 = \frac{1}{\jmath\omega C}$ and $Z_2 = \jmath\omega L$, therefore (5.15) becomes:

$$Z_o = \sqrt{\frac{L}{C}} \left(1 - \frac{1}{4\omega^2 LC}\right)^{\frac{1}{2}} \tag{5.16}$$

At cut-off frequency $\frac{1}{4\omega^2 LC} = 1$ and the circuit elements can be determined by:

$$L = \frac{Z_o}{2\omega_o} \tag{5.17}$$

$$C = \frac{1}{2Z_o\omega_o} \tag{5.18}$$

where angular cut-off frequency $\omega_o = 2\pi f_o$ and $Z_o = 50\Omega$. Assuming that the T-section in Figure 5.10 (b) is derived from Figure 5.10 (a) by a factor m, and has an input impedance $Z_{in}\prime$, that is equal to Z_{in} of T-section A, that is [57]

$$\sqrt{Z_1\prime Z_2\prime \left(1 + \frac{Z_1\prime}{4Z_2\prime}\right)} = \sqrt{Z_1 Z_2 \left(1 + \frac{Z_1}{4Z_2}\right)} \tag{5.19}$$

Then $Z_2\prime$ can be determined as:

$$Z_2\prime = \frac{1}{Z_1\prime}\left(Z_1 Z_2 + \frac{Z_1^2 - Z_1\prime^2}{4}\right) \tag{5.20}$$

Assuming that $Z_1\prime = mZ_1$, then $Z_2\prime$ can be found as:

$$Z_2\prime = \frac{Z_2}{m} + \left(\frac{1 - m^2}{4m}\right) Z_1 \tag{5.21}$$

For a highpass filter, the corresponding values for $Z_1\prime$ and $Z_2\prime$ will be:

$$Z_1\prime = \frac{m}{\jmath\omega C} \tag{5.22}$$

$$Z_2\prime = \frac{\jmath\omega L}{m} + \frac{1}{\jmath\omega C}\left(\frac{1-m^2}{4m}\right) \tag{5.23}$$

The propagation factor of the T-network can be found as:

$$\cosh(\gamma) = 1 + \frac{Z_1}{2Z_2} \tag{5.24}$$

Substituting (5.22) and (5.23) into (5.24), we get:

$$\cosh(\gamma) = \frac{\omega^2 - \omega_o^2}{\omega^2 - (1-m^2)\omega_o^2} \tag{5.25}$$

If $\omega^2 = (1-m^2)(\omega_o^2)$=$\omega_\infty$, then $\cosh(\gamma) = \infty$ implying infinite attenuation and is caused by the resonance of the series LC in the shunt arm of the T-network [56] . This condition sharpens the attenuation at cut-off frequency and the value of m can be determined as:

$$m = \sqrt{1 - \left(\frac{f_\infty}{f_o}\right)^2} \tag{5.26}$$

The frequency at at which infinite attenuation occurs f_∞, is chosen to be less than the cut-off frequency with a small variation so as not to attenuate the signal at the cut-off frequency. The resultant Figure 5.10(b) network improves on the signal attenuation rate at cut-off before cut-off frequency as compared to that of Figure 5.10 (a) network [57]. It also maintains a constant input impedance at its pass-band. The resultant T-network for T-section Figure 5.10(b) with the element configuration is as depicted in Figure 5.11. The equivalent circuits parameters are given as:

$$C_1\prime = \frac{2C}{m} \tag{5.27}$$

$$C_2\prime = \frac{4m}{1-m^2} \tag{5.28}$$

$$L_2\prime = \frac{L}{m} \tag{5.29}$$

where the values of L and C are equal to those obtained from (5.17) and (5.18). In order to incorporate the T-network in Figure 5.11 at both the transmitter and the receiver, it

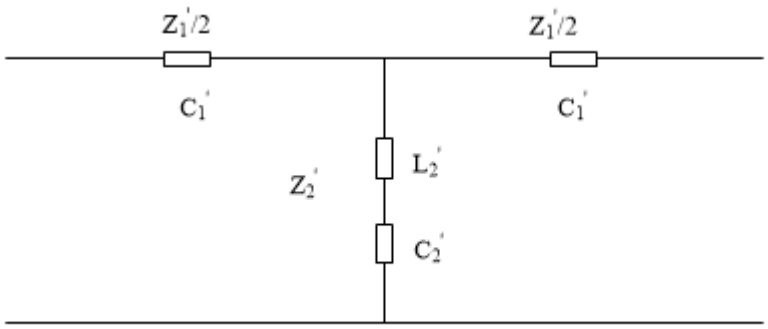

Figure 5.11: Equivalent circuit with component parameters

Figure 5.12: Bisected Pi-network

is cascaded with a similar T-network and their shunt arms are split to form a Pi-network as shown in Figure 5.12. The resulting input impedance of the Pi-network will be a function of constant m, to the corresponding T-section Figure 5.10 (a) network. For the Pi-network, m is chosen to be 0.6 in order to maintain a constant impedance over 90% of the pass-band [57], [56]. The Pi-network is then bisected and connected to either side of the matching circuit to filter out the 50 Hz mains voltage. The equivalent component parameters for the input and the out ports of the bisected Pi-network can be determined as [56]:

$$C_1'' = \frac{2C}{m} \tag{5.30}$$

$$C_2'' = \frac{2m}{1-m^2} \tag{5.31}$$

$$L_2'' = \frac{2L}{m} \tag{5.32}$$

Assuming that $Z_o = 50\ \Omega$ and the cut-off frequency is 1 MHz, f_∞ will be 800 kHz, the values for each T-section in Figure 5.11 are obtained as $C_1'' = 6.63\ nF$, $C_2\prime = 3.73\ nF$ and $L_2\prime = 16.58\ \mu H$. The T-section coupler is then integrated together with the matching circuit and the resultant circuit is as shown in Figure 5.13. The values of capacitors and inductance chosen for implementation should be as close as practically possible to the calculated values in order to minimize errors. It is also important to consider the 220 RMS

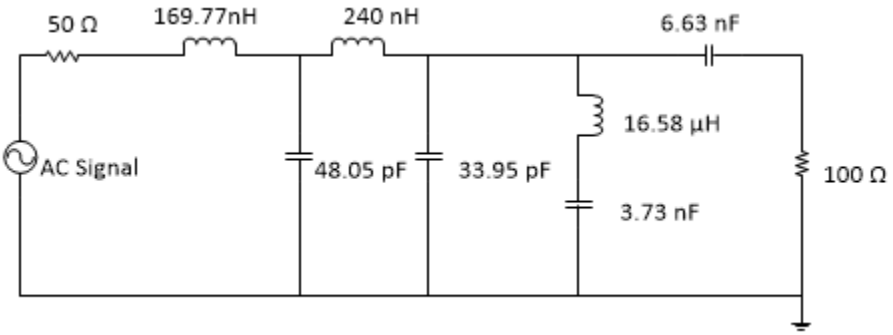

Figure 5.13: Complete matching coupler

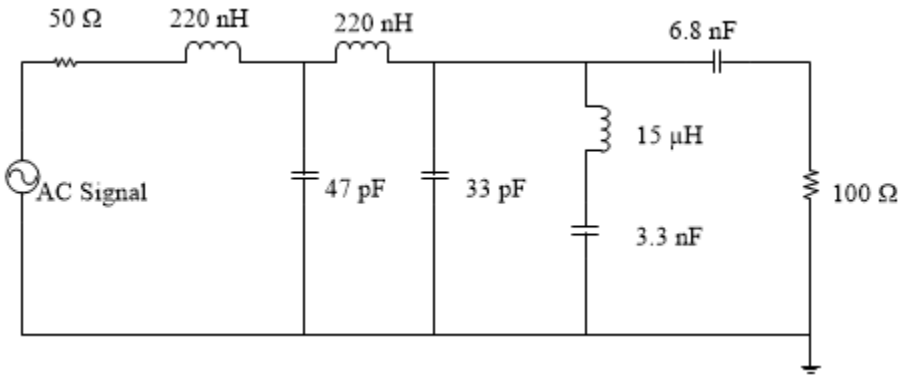

Figure 5.14: Equivalent circuit with practical component parameters

voltage at 50 Hz from the mains supply so as to use components that can withstand this voltage. For the capacitors, the maximum voltage rating can be determined through the voltage divider rule. The current across each inductor can be found by dividing the voltage calculated across each inductor by its impedance at 50 Hz [95]. The equivalent circuit with the practical component values is as shown in Figure 5.14

5.4 Results and Discussion

The performance of the coupler was evaluated using a TR5048 vector network analyzer where measurements were performed in the frequency range of 1–30 MHz. The reference port impedance for the network analyser is 50 Ω. Simulation results for the transfer function for the matching coupler for both the calculated and practical component parameters are as shown in Figure 5.15. The gain of the coupler with practical values is above the -3 dB cut-off even with the variation in the component parameters. The

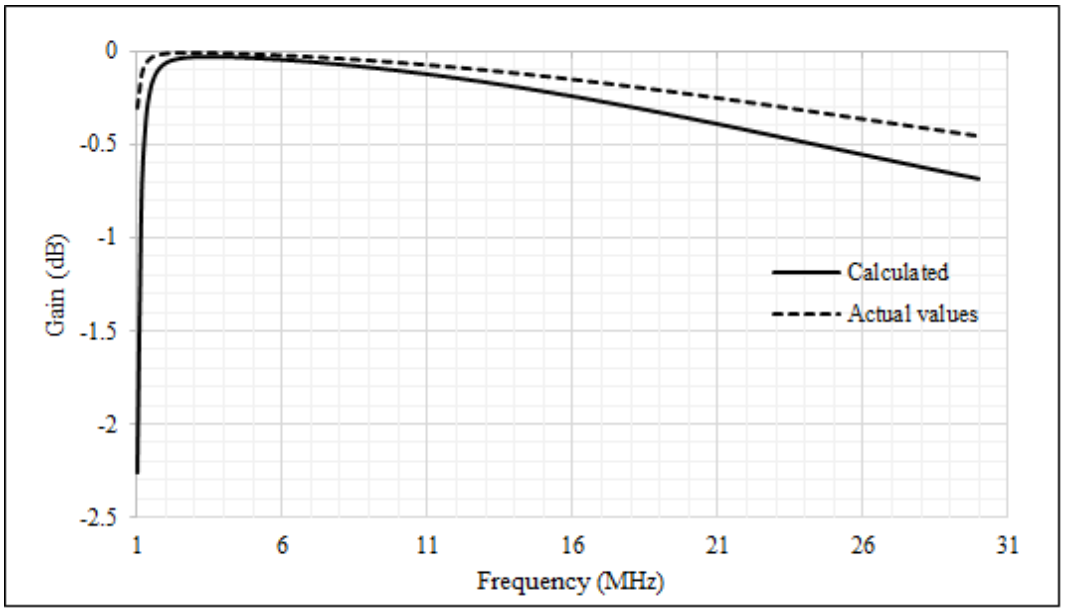

Figure 5.15: Simulated Coupler Transfer Function

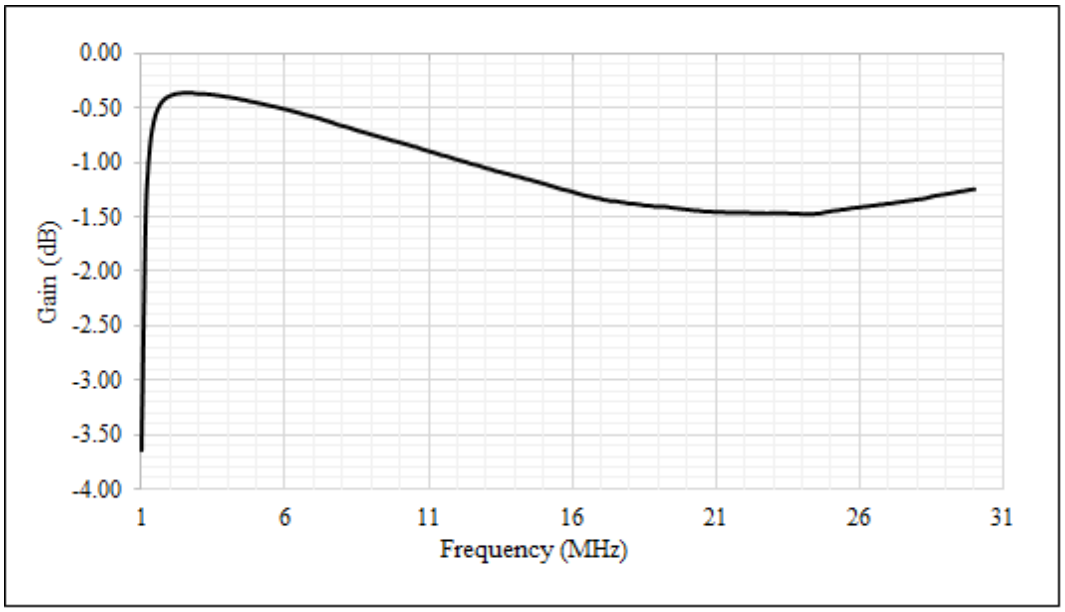

Figure 5.16: Measured Coupler Transfer Function

measurement results for the matching coupler are as depicted in Figure 5.16 where the gain is seen to decrease as the frequency approaches the upper cut-off frequency but is well above the -3 dB cut-off point for the entire band of consideration.

The simulation and the measurement results for the matching circuit with different loads are shown in Figure 5.17 and Figure 5.18, respectively. From Figure 5.18, it is observed that as the load increases from 100 Ω to 1500 Ω, the bandwidth also increases. The bandwidth for the 100 Ω load is at 5 MHz and is seen to increase to 26 MHz when the load is increased to 352 Ω as shown Figure 5.18. An even wider matching bandwidth is observed for a 1000 Ω load with an upper-cut-off frequency of 29 MHz from the measurement results. The same trend is again seen with the simulation results as depicted in Figure 5.17. The bandwidth for the 100 Ω load is seen to be narrow and the attenuation is high. This is due to the component parameters used which would be more suitable for a larger load. Since the circuit is designed for a larger load and a smaller source, the 100 Ω load is further reduced to a smaller value and thus the low gain.

The gain is also seen to improve as the load increases as seen in Figs. 5.17 and 5.18. For a frequency of 21 MHz, the gain is -5.9 dB, -2.78 dB, -2.66 dB, -2.24 dB, -1.68 dB and -1.4 dB for the 100 Ω , 330 Ω, 350 Ω, 500 Ω, 1000 Ω and 1500 Ω loads respectively as depicted in the measurement results in Figure 5.18. The coupler is thus seen to maintain a gain above the -3 dB cut-off for the changing loads from 330 Ω to 1500 Ω.

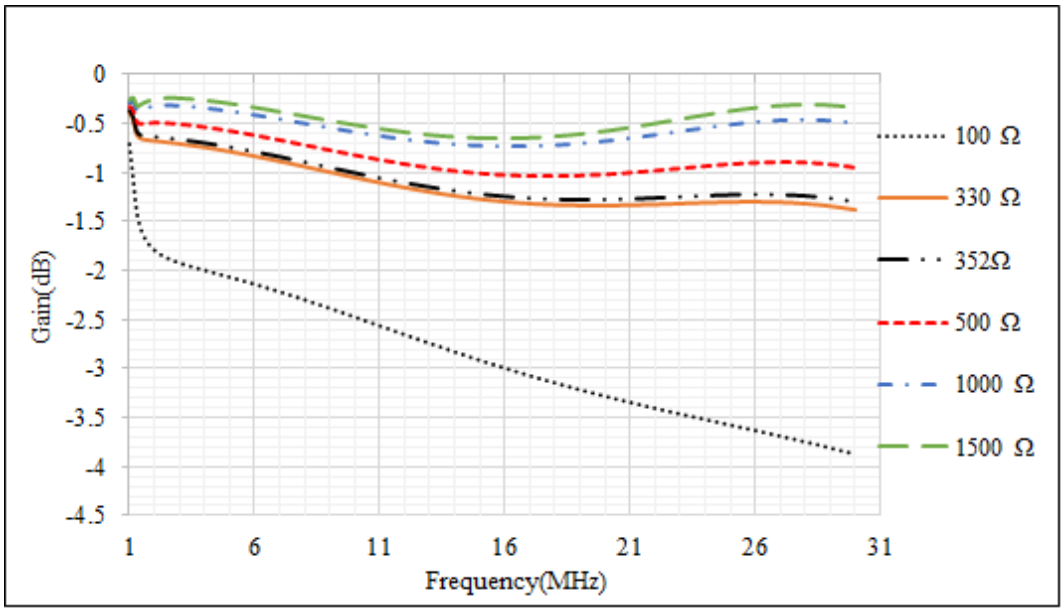

Figure 5.17: Simulation results for different loads

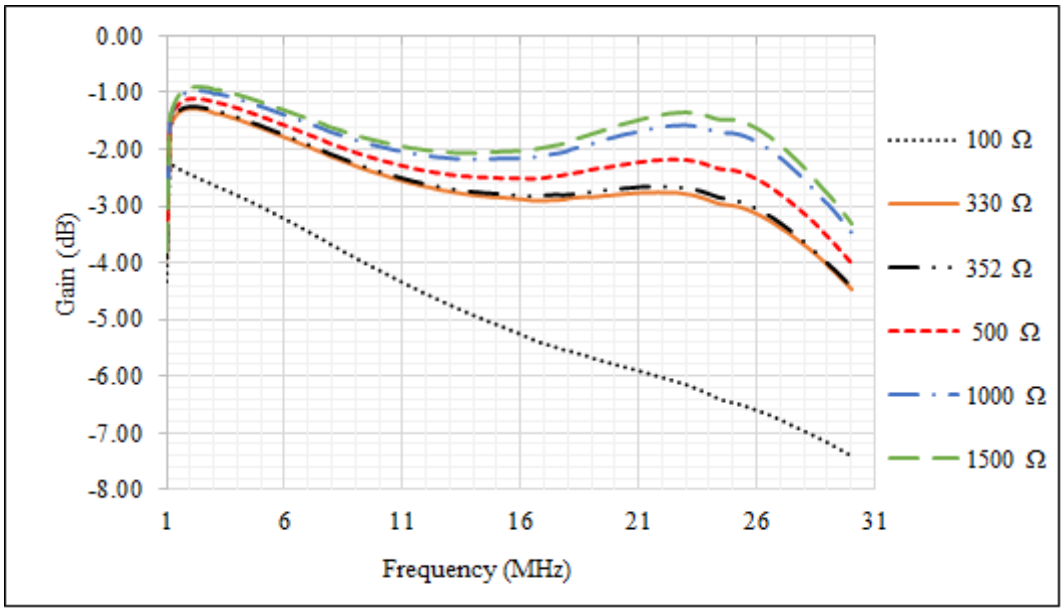

Figure 5.18: Measurement results for different loads

5.5 Summary

In this chapter, the design and implementation of a broadband matching coupler for PLC has been presented. Impedance matching is achieved through conjugate matching approach using passive filters. The matching circuit is designed as a lowpass filter which is then coupled with a highpass filter to form a bandpass filter. Thus, the unwanted signals with frequencies outside the band are filtered out. The highpass coupling section filters out the mains supply voltage preventing damage of equipment. From the measurements obtained, the matching coupler performs well with loads from 330 Ω to 1500 Ω where it maintains a constant gain of above -3 dB despite the change in loads. One of the main challenges of PLC networks is the fluctuation in the network impedance due to the loads connected and disconnected from the network resulting in impedance mismatch and high signal reflection. The coupler designed may be used to match the impedance at the bandwidth of interest. The coupler also allows for a wider matching-band since the matching section has lowpass characteristics and the coupler is highpass unlike the bandwidth achieved by using bandpass matching circuits.

Chapter 6

CONCLUSIONS AND FUTURE DEVELOPMENTS

PLC communication is gaining much popularity especially with the development of the smart grid supported by the move towards more eco-friendly technologies. Even before the introduction of the wireless network technologies, the use of PLC had began where it was employed for automatic meter reading. A lot of research is being carried out on the use of PLC to provide telecommunication services in order to meet the ever increasing demand. It has the advantage of its already in place ubiquitous infrastructure and economical establishment as it utilizes the electrical network on the upcoming infrastructures.
PLC technology like any other telecommunication technology has its challenges. These challenges include varying network impedance, considerable noise and high signal attenuation. These impairments are as a result of the power line channel design that is well suited for low frequency high voltage applications true to its original purpose. PLC on the other hand, employs the same channel to transfer high frequency communication signals, hence the hostility presented. The work presented in this dissertation seeks to model the PLC impedance characteristics so as to mitigate signal attenuation in the channel caused high signal reflection. An adaptive matching coupler is designed to that effect to extend its application beyond protection of communication devices from high voltages.

6.1 Summary of Results

- Various modelling techniques of the power line channel have been reviewed in chapter 2 where they have been categorised into two groups; top-down and bottom-up approach. The bottom-up approach requires the background knowledge of the PLC channel characteristics calling for the extraction of the line parameters. This is performed in chapter 3 where the two methods of line parameter extraction have been disscussed, that is, the theorectical and the measurement based approaches. For the theoretical approach, the distributed parameters are first determined from which the characteristic impedance and the propagation constant, essential in the deterministic channel modelling, are determined. For the measurement approach, input impedances for both the short-circuit and open-circuit terminations are determined. The characteristic impedance, propagation constant and the distributed line parameters are then determined from the measured results under the open and short-circuit load conditions. The line parameters results using both approaches are

plotted on the same set of axis and show a good agreement.

- The input impedance of the PLC channel is modeled in chapter 4 using the parallel resonant circuit model by applying the transmission line theory for a two conductor transmission line. From the measurements carried out for known PLC network topologies, the model shows a good agreement with the measurements. Measurements were also performed for different branch lengths and different number of branches. The results show that the branch lengths are responsible for the number of peaks in the bandwidth of interest. It is also observed that impedance peaks begin occurring at lower frequencies for longer branches as compared to shorter branches. When the number of branches are increased, the magnitude of the peaks also increases. The measurements also verified that for branches of the same length, the peaks will occur at the same resonant frequencies albeit stronger. The impedance measurement results were then characterized and profiled into minimum, average and maximum values for the different network topologies. It was observed that for single branched networks, the average value of the input impedance is approximately the same with a value of 354 $\pm$ 1.1 % Ω. However, when the number of branches is increased, the average impedance values vary. It is also observed that the maximum peaks do fluctuate randomly and do not depend on either the branch length or the number of branches. The results obtained are important in the modeling of the PLC transfer function as well as in the design of impedance matching circuits in PLC modems.

- Through findings in the behavior of the network impedance, an impedance matching coupler is designed in chapter 5. From measurement tests the coupler is seen to exhibit bandpass characteristics effected by the design where the coupling section is designed as a high pass filter and the the matching circuit designed as a lowpass filter. The prototype matching coupler was tested using different loads connected to the PLC network. The measurement results show that the designed coupler performs very well for impedances starting from 150 Ω and improves a great deal as the impedance increases. The measurements show that impedance is matched for almost the entire frequency band for higher input impedances . However, for lower impedances the level of matching is low.

6.2 Future Research Work

From the investigations carried out in this dissertation, the PLC network is confirmed to have an input impedance that varies randomly with frequency. The matching coupler designed only uses passive filters and thus this work can further be extended and improved in order to to have a more friendly medium for the transfer of communication signal as follows:

- From the input impedance measurements, more research campaigns need to be

carried out especially on the broadband PLC. This measurement campaign should encompass unknown network topologies in different indoor environments such as offices, homes, laboratories and industrial set-ups. Since the wiring practices vary from country to country, various measurement campaigns on the PLC network impedance need to be carried out especially in the African continent as the measurements available currently are from other parts of the world.

- From the measurements, obtained from the designed coupler, it is observed that at low impedance values, the impedance matching is low and therefore further research can be done so as to extend the impedance matching to lower impedance values. The protective circuitry that encompasses zener diodes, coupling transformers and transient voltage suppressors calls for further research so as to incorporate it to the matching coupler.
- With the development of the smart grid and home automation, the investigation and design of smart couplers that can detect the input impedance values and match accordingly can be done for future PLC applications.

References

[1] P. Brown, "Power line communications-past, present, and future," in *Proceedings of International Symposium on Power-line Communications and its Applications*, pp. 1–8, 1999.

[2] X. Carcelle, *Power line communications in practice*. Artech House, 2009.

[3] S. Galli, A. Scaglione, and Z. Wang, "Power line communications and the smart grid," in *Smart Grid Communications (SmartGridComm), 2010 First IEEE International Conference on*, pp. 303–308, IEEE, 2010.

[4] A. J. Snyders, P. A. J. van Rensburg, and H. C. Ferreira, "M-fsk carrier gain adjustment for improved power-line communications," *IEEE Transactions on Power Delivery*, vol. 25, no. 2, pp. 674–679, 2010.

[5] H. Ferreira, H. Grové, O. Hooijen, and A. Vink, "Power line communication (in wiley encyclopaedia of electrical and electronics engineering)," *New York: Wiley*, pp. 706–716, 1999.

[6] W. A. Finamore, M. V. Ribeiro, and L. Lampe, "Advancing power line communication: Cognitive, cooperative, and mimo communication," in *Brazilian Telecommunications Symposium*, pp. 13–16, 2012.

[7] L. T. Berger, A. Schwager, and J. J. Escudero-Garzás, "Power line communications for smart grid applications," *Journal of Electrical and Computer Engineering*, vol. 2013, p. 3, 2013.

[8] J. Routin and C. L. Brown, "Improvements in and relating to electricity meters," *British Patent GB*, vol. 189724, p. 833, 1898.

[9] C. H. Thordarson, "Electric central-station recording mechanism for meters.," Mar. 14 1905. US Patent 784,712.

[10] K. Dostert, *Powerline communications*. Prentice Hall PTR, 2001.

[11] S. Galli, A. Scaglione, and Z. Wang, "For the grid and through the grid: The role of power line communications in the smart grid," *Proceedings of the IEEE*, vol. 99, no. 6, pp. 998–1027, 2011.

[12] P. Tanguy and F. Nouvel, "In-vehicle plc simulator based on channel measurements," in *International conference on intelligent transport system telecommunication (ITST)*, pp. 1–5, 2010.

[13] M. S. Yousuf and M. El-Shafei, "Power line communications: An overview-part i," in *Innovations in Information Technology, 2007. IIT'07. 4th International Conference on*, pp. 218–222, IEEE, 2007.

[14] C. J. Kim and M. F. Chouikha, "Attenuation characteristics of high rate home-networking plc signals," *IEEE transactions on power delivery*, vol. 17, no. 4, pp. 945–950, 2002.

[15] M. Shwehdi and A. Khan, "A power line data communication interface using spread spectrum technology in home automation," *IEEE Transactions on Power Delivery*, vol. 11, no. 3, pp. 1232–1237, 1996.

[16] M. Schwartz, "Carrier-wave telephony over power lines: Early history [history of communications]," *IEEE Communications Magazine*, vol. 47, no. 1, pp. 14–18, 2009.

[17] M. Schwartz, "The origins of carrier multiplexing: Major george owen squier and at&t," *IEEE Communications Magazine*, vol. 46, no. 5, 2008.

[18] N. Marumo, "Simultaneous transmission and reception in radio telephony," *Proceedings of the Institute of Radio Engineers*, vol. 8, no. 3, pp. 199–219, 1920.

[19] B. Kleebinder, "Die hochfrequenztelephonie für elektrizitatswerke," *Elektrotechnik und Maschinenbau*, vol. 46, no. 36, 1929.

[20] H.-K. Podszeck, *Carrier communication over power lines*, vol. 80. Springer, 1972.

[21] J. Nevel, "History and theory of ripple communication system," in *Proc. Nat. Telecommun. Conf.*, pp. 2–3, 1976.

[22] H. C. Ferreira, L. Lampe, J. Newbury, and T. G. Swart, *Power line communications: theory and applications for narrowband and broadband communications over power lines*. John Wiley & Sons, 2011.

[23] N. Pavlidou, A. H. Vinck, J. Yazdani, and B. Honary, "Power line communications: state of the art and future trends," *IEEE Communications magazine*, vol. 41, no. 4, pp. 34–40, 2003.

[24] C. EN50065, "1, signaling on low voltage electrical installations in the frequency range 3 khz to 148, 5 khz," *CENELEC, Bruxelles, Belgique*, 2002.

[25] H. Meng, S. Chen, Y. Guan, C. Law, P. So, E. Gunawan, and T. Lie, "Modeling of transfer characteristics for the broadband power line communication channel," *IEEE Transactions on power delivery*, vol. 19, no. 3, pp. 1057–1064, 2004.

[26] P. Brown, "High frequency conditioned power networks," in *UTC Annu. Conf. Proc*, 1995.

[27] J. Adami, P. Silveira, M. Martinez, R. Perez, and A. Dallbello, "New approach to improve high-voltage transmission line reliability," *IEEE Transactions on Power Delivery*, vol. 24, no. 3, pp. 1515–1520, 2009.

[28] A. Cataliotti, A. Daidone, and G. Tinè, "Power line communication in medium voltage systems: characterization of mv cables," *IEEE Transactions on Power Delivery*, vol. 23, no. 4, pp. 1896–1902, 2008.

[29] P. Strong, "Regulatory & consumer acceptance of powerline products," in *Proceedings of the 5th International Symposium on Power-Line Communications and its Applications (ISPLC)*, pp. 4–6, 2001.

[30] A. R. Ndjiongue, A. Snyders, H. C. Ferreira, and S. Rimer, "Review of power line communications standards in africa," in *International Conference on e-Infrastructure and e-Services for Developing Countries*, pp. 12–21, Springer, 2013.

[31] A. M. Tonello and A. Pittolo, "Considerations on narrowband and broadband power line communication for smart grids," in *Smart Grid Communications (SmartGridComm), 2015 IEEE International Conference on*, pp. 13–18, IEEE, 2015.

[32] J. Auvray and M. Fourrier, *Problems in electronics (including lumped constants, transmission lines, and high frequencies)*, vol. 61. Pergamon, 1973.

[33] O. G. Hooijen, "On the relation between network-topology and power line signal attenuation," in *ISPLC*, vol. 98, pp. 24–26, 1998.

[34] D. Chffanjon, "Electric de france a real knowledge for propagation: the way of efficiency and reliability making plc generalization feasible," in *ISPLC-98 Proceedings*, pp. 57–66.

[35] M. H. Chan and R. W. Donaldson, "Attenuation of communication signals on residential and commercial intrabuilding power-distribution circuits," *IEEE Transactions on Electromagnetic compatibility*, vol. 28, no. 4, pp. 220–230, 1986.

[36] P. Favre, C. Candolfi, M. Schneider, M. Rubinstein, P. Krahenbuehl, and A. Vukicevic, "Common mode current and radiations mechanisms in plc networks," in *Power Line Communications and Its Applications, 2007. ISPLC'07. IEEE International Symposium on*, pp. 348–354, IEEE, 2007.

[37] E. Marthe, F. Rachidi, M. Ianoz, and P. Zweiacker, "Indoor radiated emission associated with power line communication systems," in *Electromagnetic Compatibility, 2001. EMC. 2001 IEEE International Symposium on*, vol. 1, pp. 517–520, IEEE, 2001.

[38] R. Vick, "Radiated emission caused by in-house plc-systems," in *Proc. 2001 ISPLC Conf*, pp. 197–202, 2001.

[39] P. Mlynek, J. Misurec, M. Koutny, and R. Fujdiak, "Transfer function of power line channelâĂŤinfluence of topology parameters and power line topology estimation," in *Innovative Smart Grid Technologies Conference Europe (ISGT-Europe), 2014 IEEE PES*, pp. 1–5, IEEE, 2014.

[40] B. Masood and S. Baig, "Channel modeling of nb-plc for smart grid," in *Computers and Communication (ISCC), 2015 IEEE Symposium on*, pp. 745–750, IEEE, 2015.

[41] M. Korki, N. Hosseinzadeh, H. L. Vu, T. Moazzeni, and C. H. Foh, "A channel model for power line communication in the smart grid," in *Power Systems Conference and Exposition (PSCE), 2011 IEEE/PES*, pp. 1–7, IEEE, 2011.

[42] P. J. Langfeld and K. Dostert, "The capacity of typical powerline reference channels and strategies for system design," in *International Symposium on Power-Line Communications and its Applications (ISPLC)*, pp. 271–278, 2001.

[43] M. Zimmermann and K. Dostert, "A multipath model for the powerline channel," *IEEE Transactions on communications*, vol. 50, no. 4, pp. 553–559, 2002.

[44] H. Meng, S. Chen, Y. Guan, C. Law, P. So, E. Gunawan, and T. Lie, "A transmission line model for high-frequency power line communication channel," in *Power System Technology, 2002. Proceedings. PowerCon 2002. International Conference on*, vol. 2, pp. 1290–1295, IEEE, 2002.

[45] K. Khalil, M. G. Gazalet, F.-X. Coudoux, P. Corlay, and M. Gharbi, "Random channel transfer function generation for broadband indoor mimo plc," in *Power Line Communications and its Applications (ISPLC), 2016 International Symposium on*, pp. 87–92, IEEE, 2016.

[46] J. A. Corchado, J. A. Cortés, F. J. Canete, and L. Díez, "An mtl-based channel model for indoor broadband mimo power line communications," *IEEE Journal on Selected Areas in Communications*, vol. 34, no. 7, pp. 2045–2055, 2016.

[47] H. Philipps, "Modelling of powerline communication channels," in *Proc. 3rd IntâĂŹl. Symp. Power-Line Commun. and its Applications*, pp. 14–21, 1999.

[48] J. Anatory, M. Kissaka, and N. Mvungi, "Channel model for broadband power-line communication," *IEEE transactions on power delivery*, vol. 22, no. 1, pp. 135–141, 2007.

[49] J. Anatory and N. Theethayi, *Broadband power-line communications systems: theory & applications*. wit press, 2010.

[50] F. Zwane and T. J. Afullo, "An alternative approach in power line communication channel modelling.," *Progress In Electromagnetics Research C*, vol. 47, 2014.

[51] M. Mosalaosi and T. Afullo, "A deterministic channel model for multi-access broadband powerline communication," in *AFRICON, 2015*, pp. 1–5, IEEE, 2015.

[52] S. O. Awino, "Alternative approach to power line communication (plc) channel modelling and multipath characterization," Master's thesis, University of KwaZulu-Natal, Durban, 2016.

[53] J. Anatory, N. Theethayi, R. Thottappillil, M. Kissaka, and N. H. Mvungi, "The influence of load impedance, line length, and branches on underground cable power-line communications (plc) systems," *IEEE Transactions on Power Delivery*, vol. 23, no. 1, pp. 180–187, 2008.

[54] T. Esmailian, F. Kschischang, and P. Gulak, "An in-building power line channel simulator," in *International Symposium on Power Line Communications and Its Applications (ISPLC)*, pp. 27–29, 2002.

[55] M. Zimmermann and K. Dostert, "A multi-path signal propagation model for the power line channel in the high frequency range," in *Proceedings of the 3rd International Symposium on Power-Line Communications, Lancaster, UK*, vol. 30, 1999.

[56] D. M. Pozar, *Microwave engineering 4e.* John Wiley & Sons, 2012.

[57] D. Misra, *Radio-frequency and microwave communication circuits: analysis and design.* John Wiley & Sons, 2004.

[58] M. N. Sadiku, *Elements of electromagnetics.* Oxford university press, 2014.

[59] J. Nguimbis, S. Cheng, Y. Zhang, and L. Xiong, "Coupling unit topology for optimal signaling through the low-voltage powerline communication network," *IEEE Transactions on Power Delivery*, vol. 19, no. 3, pp. 1065–1071, 2004.

[60] T. Banwell and S. Galli, "A novel approach to the modeling of the indoor power line channel part i: circuit analysis and companion model," *IEEE Transactions on power delivery*, vol. 20, no. 2, pp. 655–663, 2005.

[61] T.-E. Sung, A. Scaglione, and S. Galli, "Time-varying power line block transmission models over doubly selective channels," in *Power Line Communications and Its Applications, 2008. ISPLC 2008. IEEE International Symposium on*, pp. 193–198, IEEE, 2008.

[62] M. P. Sibanda, P. A. J. van Rensburg, and H. C. Ferreira, "Impedance matching with low-cost, passive components for narrowband plc," in *Power Line Communications and Its Applications (ISPLC), 2011 IEEE International Symposium on*, pp. 335–340, IEEE, 2011.

[63] M. De Piante and A. M. Tonello, "On impedance matching in a power-line-communication system," *IEEE Transactions on Circuits and Systems II: Express Briefs*, vol. 63, no. 7, pp. 653–657, 2016.

[64] R. Joshi, H. Jadav, A. Mali, and S. Kulkarni, "Integration of plc based offline impedance matching system for icrh experiments," in *Contemporary Computing and Informatics (IC3I), 2016 2nd International Conference on*, pp. 564–567, IEEE, 2016.

[65] P. A. J. van Rensburg, M. P. Sibanda, and H. C. Ferreira, "Integrated impedance-matching coupler for smart building and other power-line communications applications," *IEEE Transactions on Power Delivery*, vol. 30, no. 2, pp. 949–956, 2015.

[66] P. J. van Rensburg, A. Snyders, and H. Ferreira, "Complementary capacitive-inductive data coupler for power-line communications," *Australian Patent*, no. 2011101421, 2011.

[67] L. Qi, S. Jingzhao, and F. Zhenghe, "Adaptive impedance matching in power line communication," in *Microwave and Millimeter Wave Technology, 2004. ICMMT 4th International Conference on, Proceedings*, pp. 887–890, IEEE, 2004.

[68] W.-h. Choi and C.-y. Park, "A simple line coupler with adaptive impedance matching for power line communication," in *Power Line Communications and Its Applications, 2007. ISPLC'07. IEEE International Symposium on*, pp. 187–191, IEEE, 2007.

[69] C.-Y. Park, K.-H. Jung, and W.-H. Choi, "Coupling circuitary for impedance adaptation in power line communications using vcgic," in *Power Line Communications and Its Applications, 2008. ISPLC 2008. IEEE International Symposium on*, pp. 293–298, IEEE, 2008.

[70] I. C. Papaleonidopoulos, C. G. Karagiannopoulos, N. J. Theodorou, and C. N. Capsalis, "Theoretical transmission-line study of symmetrical indoor triple-pole cables for single-phase hf signalling," *IEEE transactions on power delivery*, vol. 20, no. 2, pp. 646–654, 2005.

[71] I. C. Papaleonidopoulos, C. N. Capsalis, C. G. Karagiannopoulos, and N. J. Theodorou, "Statistical analysis and simulation of indoor single-phase low voltage power-line communication channels on the basis of multipath propagation," *IEEE Transactions on Consumer Electronics*, vol. 49, no. 1, pp. 89–99, 2003.

[72] F. Zwane, *Power Line Communication Channel Modelling*. PhD thesis, Citeseer, 2014.

[73] G. T. Andreou and D. P. Labridis, "Electrical parameters of low-voltage power distribution cables used for power-line communications," *IEEE Transactions on Power delivery*, vol. 22, no. 2, pp. 879–886, 2007.

[74] C. R. Paul, *Analysis of multiconductor transmission lines*. John Wiley & Sons, 2008.

[75] C. Hensen, W. Schulz, and S. Schwarze, "Characterization measurement and modeling of medium-voltage power line cables for high data rate communication," in *proc International Symposium on Power Line Communications and Its Applications*, 1999.

[76] E. J. Bartolucci and B. H. Finke, "Cable design for pwm variable-speed ac drives," *IEEE Transactions on Industry Applications*, vol. 37, no. 2, pp. 415–422, 2001.

[77] W. Tomasi, *Electronic communications systems: fundamentals through advanced*. Prentice Hall PTR, 1987.

[78] J. Huloux and L. Hanus, "St7537 power line modem application," *ST Microelectronics*, 1995.

[79] G. Laguna and R. Barron, "Survey on indoor power line communication channel modeling," in *Electronics, Robotics and Automotive Mechanics Conference, 2008. CERMA'08*, pp. 163–168, IEEE, 2008.

[80] H. Philipps, "Performance measurements of powerline channels at high frequencies," in *Proceedings of the International Symposium on Power Line Communications and its Applications (ISPLC)*, vol. 229237, 1998.

[81] S. Tsuzuki, T. Takamatsu, H. Nishio, and Y. Yamada, "An estimation method of the transfer function of indoor power-line channels for japanese houses," in *Proc. Int. Symp. Power-Lines Commun*, pp. 55–59, 2002.

[82] H. Tian, R. Yuan, F. Li, Z. Huang, S. Wang, S. Li, and K. Zhong, "Measurement on narrow band power line communication channel impedance of distribution network," in *Consumer Electronics, Communications and Networks (CECNet), 2011 International Conference on*, pp. 454–457, IEEE, 2011.

[83] B. Rasool, A. Rasool, and I. Khan, "Impedance characterization of power line communication networks," *Arabian Journal for Science and Engineering*, vol. 39, no. 8, pp. 6255–6267, 2014.

[84] M. Tanaka, "High frequency noise power spectrum, impedance and transmission loss of power line in japan on intrabuilding power line communications," *IEEE Transactions on Consumer Electronics*, vol. 34, no. 2, pp. 321–326, 1988.

[85] J. Nicholson and J. Malack, "Rf impedance of power lines and line impedance stabilization networks in conducted interference measurements," *IEEE Transactions on Electromagnetic Compatibility*, no. 2, pp. 84–86, 1973.

[86] R. M. Vines, H. J. Trussell, K. C. Shuey, and J. B. O'Neal, "Impedance of the residential power-distribution circuit," *IEEE Transactions on Electromagnetic Compatibility*, no. 1, pp. 6–12, 1985.

[87] I. H. Cavdar and E. Karadeniz, "Measurements of impedance and attenuation at CENELEC bands for power line communications systems," *Sensors*, vol. 8, no. 12, pp. 8027–8036, 2008.

[88] F Chelangat, TJO Afullo, M Mosalaosi, "Impedance Modelling, Profiling and Characterisation of the Powerline Communication Channel," *Proceedings of Progress in Electromagnetics Research Symposium (PIERS) 2018, Toyama, Japan, 1-4 August, 2018*, pp.2165-2171.

[89] A. A. Smith, *Radio Frequency Principles & Applications*. Universities Press, 1998.

[90] B. Martinez, N. Cante, M. Limas, F. Sierra, and J. Becerra, "Design of a t-coupling circuit for plc on broadband," in *Communications and Computing (COLCOM), 2014 IEEE Colombian Conference on*, pp. 1–6, IEEE, 2014.

[91] M. P. Sibanda, P. A. J. van Rensburg, and H. C. Ferreira, "Passive, transformerless coupling circuitry for narrow-band power-line communications," in *Power Line Communications and Its Applications, 2009. ISPLC 2009. IEEE International Symposium on*, pp. 125–130, IEEE, 2009.

[92] O. G. Hooijen, "A channel model for the residential power circuit used as a digital communications medium," *IEEE transactions on electromagnetic compatibility*, vol. 40, no. 4, pp. 331–336, 1998.

[93] D. Anastasiadou and T. Antonakopoulos, "An experimental setup for characterizing the residential power grid variable behavior," in *Proc. 2002 of the 6th International Symposium on Power-Line Communications and its Applications*, 2002.

[94] J. B. Hagen, *Radio-frequency electronics: circuits and applications*. Cambridge University Press, 2009.

[95] M. P. Sibanda, P. A. J. van Rensburg, and H. C. Ferreira, "A compact economical plc band-pass coupler with impedance matching," in *Power Line Communications and Its Applications (ISPLC), 2013 17th IEEE International Symposium on*, pp. 339–344, IEEE, 2013.